ELSEVIER

Chemical Geology 237 (2007) 23–45

CHEMICAL GEOLOGY
INCLUDING
ISOTOPE GEOSCIENCE

www.elsevier.com/locate/chemgeo

# Stratigraphy and geochemistry of a ca 800 Ma negative carbon isotope interval in northeastern Svalbard

Galen P. Halverson [a,*], Adam C. Maloof [b], Daniel P. Schrag [c], Francis Ö. Dudás [d], Matthew Hurtgen [e]

[a] UMR 5563, LMTG-IRD-CNRS, Université Toulouse-3, 14 avenue Edouard Belin, 31400 Toulouse, France
[b] Department of Geosciences, Princeton University, Guyot Hall, Princeton, NJ 08544, USA
[c] Department of Earth and Planetary Sciences, Harvard University, 20 Oxford St., Cambridge, MA 02138, USA
[d] Department of Earth, Atmospheric, and Planetary Sciences, MIT, Building 54-1124, Cambridge, MA 02139, USA
[e] Department of Geological Sciences, Northwestern University, 1850 Campus Dr., Evanston, IL 60208, USA

Accepted 8 June 2006

Editor: P. Dienes

**Abstract**

The Neoproterozoic Akademikerbreen Group in northeastern Svalbard comprises 2 km of nearly pure carbonate section. The carbonates are generally highly $^{13}$C-enriched ($\delta^{13}C > 5‰$), but this trend is interrupted by an ~325 m interval of low $\delta^{13}C$ values (−4 to 0‰) in the upper Grusdievbreen and lower Svanbergfjellet formations. An abrupt negative isotopic shift at the onset of this low $\delta^{13}C$ interval is reproduced in detail in multiple sections along the length of the outcrop belt (125 km) and everywhere coincides with a prominent sequence boundary and change in lithology. Likewise, the return to positive $\delta^{13}C$ values coincides with a second exposure surface. Correlation of the lower Akademikerbreen Group $\delta^{13}C$ record with a nearly identical isotopic profile in the Bitter Springs Formation of Central Australia suggests an age of ~800 Ma for the low $\delta^{13}C$ interval and confirms that it is a global seawater signal. The coincidence of the negative and positive $\delta^{13}C$ shifts with major stratigraphic perturbations in the otherwise conformable succession suggests that both episodes of transient sea level change were related to global phenomena. $^{87}Sr/^{86}Sr$ ratios rise transiently from an average of 0.7063 to 0.7066 within this interval. Whereas large negative $\delta^{13}C$ anomalies in the Neoproterozoic are commonly associated with episodes of widespread glaciation, the Akademikerbreen low $\delta^{13}C$ interval precedes the oldest (Sturtian) of the known Neoproterozoic glacial events, and no other evidence suggests an ice age at this time. We propose instead that the negative $\delta^{13}C$ interval is related to a pair of inertial interchange true polar wander (TPW) events.


*Keywords:* Neoproterozoic; Svalbard; Chemostratigraphy; $\delta^{13}C$; $^{87}Sr/^{86}Sr$; TPW

## 1. Introduction

The carbon-isotopic composition of the Neoproterozoic oceans was generally high, but fluctuated by at least 15‰ (Shields and Veizer, 2002) coincident with episodes of widespread glaciation (Knoll et al., 1986; Kaufman and Knoll, 1995; Kaufman et al., 1991, 1997). The highly $^{13}$C-enriched intervals typical of interglacial times have received only minor attention, but it is widely assumed that the enrichment of the oceans was a result of unusually efficient burial of organic matter in

* Corresponding author.
*E-mail address:* galen.halverson@adelaide.edu.au (G.P. Halverson).

0009-2541/$ - see front matter © 2006 Elsevier B.V. All rights reserved.
doi:10.1016/j.chemgeo.2006.06.013

Neoproterozoic ocean basins, perhaps as a consequence of high erosion rates related to widespread orogenesis and abundant nutrient availability (Derry et al., 1992; Kaufman et al., 1995). The negative $\delta^{13}C$ anomalies have received much greater attention, due in large part to their intimate relationship to glaciation (Hoffman et al., 1998a,b). Three Neoproterozoic glaciations and associated $\delta^{13}C$ anomalies have been identified (Halverson et al., 2005; Xiao et al., 2004): the oldest (Sturtian) postdates ~750 Ma and is perhaps as young as ~710 Ma (Brasier et al., 2000), the middle (Marinoan) glaciation likely ended ~635 Ma (Hoffmann et al., 2004) and the youngest (Gaskiers) was short-lived and occurred at ~580 Ma (Bowring et al., 2003; Knoll et al., 2004). The negative $\delta^{13}C$ anomalies are best known from cap–carbonate sequences to the Sturtian and Marinoan glaciations (Williams, 1979; Kennedy, 1996; Kaufman et al., 1997; Kennedy et al., 1998; Hoffman and Schrag, 2002) and had long been regarded as solely post-glacial phenomena. This assumption underlies popular cause-and-effect hypotheses for the presumed linkage between climate change and $\delta^{13}C$ patterns, but it is now apparent that the negative $\delta^{13}C$ anomalies are variable in magnitude and pattern for each of the Neoproterozoic glacial episodes (Halverson et al., 2005). Furthermore, at least one glaciation is preceded by a global negative $\delta^{13}C$ anomaly (Hoffman et al., 1998a; McKirdy et al., 2001; Halverson et al., 2002), implying a complex relationship between global climate and $\delta^{13}C$ in the Neoproterozoic (Schrag et al., 2002).

The absence of a simple cause-and-effect relationship between negative $\delta^{13}C$ excursions and glaciation raises the possibility that carbon isotope anomalies could occur independent of glaciation. Hill et al. (2000a,b) found evidence for a decoupling between Neoproterozoic $\delta^{13}C$ anomalies and glaciation when they documented a salient interval of low $\delta^{13}C$ in pre-Sturtian (~800 Ma) carbonates (Walter et al., 1995; Hill and Walter, 2000) of the Bitter Springs Formation in central Australia. We have documented what we interpret to be the same low $\delta^{13}C$ interval in the Akademikerbreen Group in northeastern Svalbard where it is defined by a sharp decline of ~8‰ in the middle Grusdievbreen Formation and a rise of similar magnitude in the lower Svanbergfjellet Formation. Both isotope shifts are associated with regionally persistent, conformable exposure surfaces and appear to represent switches between contrasting steady state conditions of carbon cycling, related to global events that caused transient fluctuations in sea level. In this paper we present detailed stratigraphic, isotopic, and elemental data spanning the Grusdievbreen and Svanbergfjellet formations to constrain possible geological processes that may have contributed to the carbon isotopic and stratigraphic patterns spanning the low $\delta^{13}C$ interval in Svalbard.

## 2. Geological background

The Svalbard archipelago consists of three tectonic terranes that were juxtaposed during the Silurian–Devonian Ny Friesland orogeny (Harland and Gayer, 1972; Harland et al., 1992; Gee and Page, 1994; Lyberis and Manby, 1999). The thick, Neoproterozoic–Ordovician middle–upper Hecla Hoek Succession (Fig. 1) underlies the northern part of the eastern terrane and is nearly identical to the Neoproterozoic succession in the southern East Greenland Caledonides, suggesting that both were deposited in a contiguous basin (East Greenland–East Svalbard — EGES platform) that was dissected during the Caledonian orogeny (Harland and Gayer, 1972). The origin of the EGES platform remains obscure, but presumably it was associated with the fragmentation of Rodinia, which in this region involved the separation of four cratons including Laurentia, Baltica, and Amazonia (Torsvik et al., 1996; Hartz and Torsvik, 2002). Paleomagnetic data indicate that the EGES platform remained in tropical latitudes throughout deposition of the Akademikerbreen Group (Maloof et al., 2006).

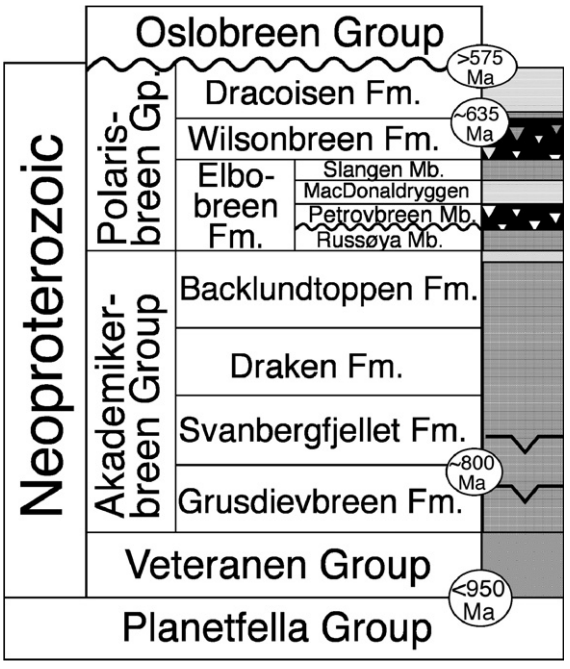


Fig. 1. Generalized lithostratigraphy of the Neoproterozoic successions in northeast Svalbard after Harland et al. (1993), Fairchild and Hambrey (1984), Knoll and Swett (1990), Halverson et al. (2005). See text for discussion of age constraints (shown in ovals).

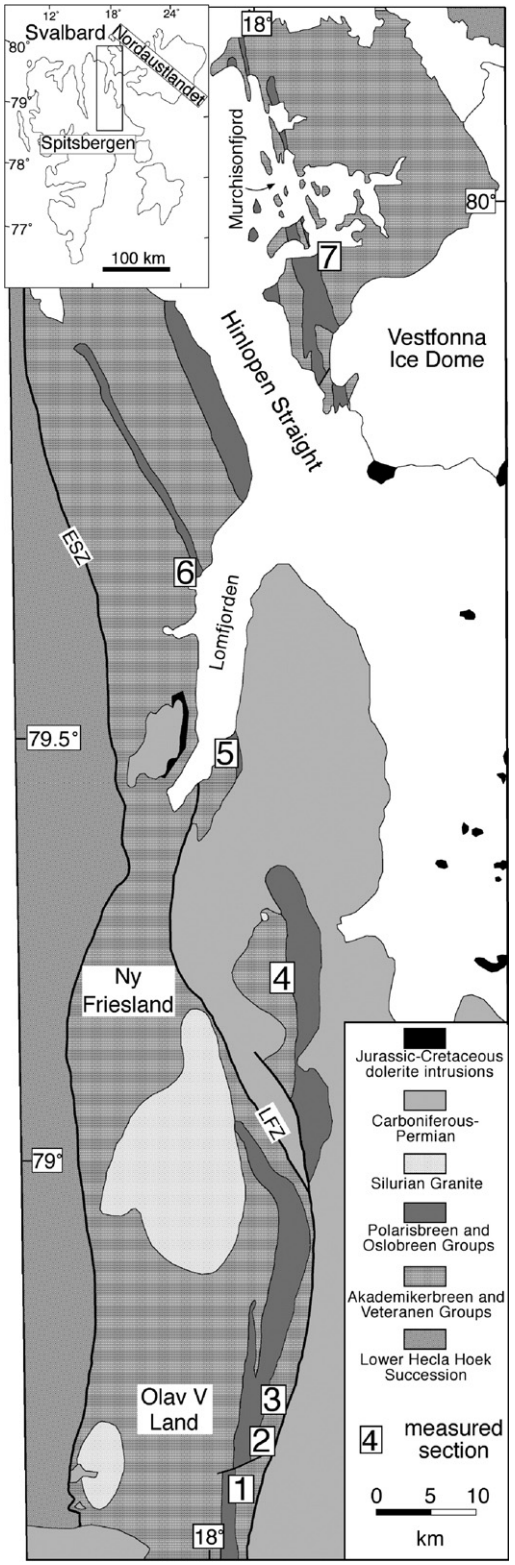


The north–south trending outcrop belt of Neoproterozoic rocks comprises up to 7 km of strata, traceable for 120 km from northern Spitsbergen to western Nordaustlandet in northeast Svalbard (Fig. 2). A different stratigraphic nomenclature is used in Spitsbergen and Nordaustlandet, but due to the unambiguous correlation of the strata between the two islands (Fairchild and Hambrey, 1995) and for the sake of simplicity, only the nomenclature from Spitsbergen is used here (Fig. 1). The ~4 km-thick Veteranen Group forms the base of the Neoproterozoic succession and consists predominantly of siliciclastic sediments, but contains three distinct carbonate units (Wilson, 1958; Knoll et al., 1986). The Veteranen Group is constrained to be younger than ~950 Ma based on U–Pb dates from magmatic zircons in basement granites in the Nordaustlandet region (Gee et al., 1995; Johannson et al., 2000) and detrital zircons in the Planetfjella Group in Ny Friesland (Larianov et al., 1998).

The Veteranen Group siliciclastic sediments are transitional with the ~2 km of nearly pure carbonate section of the Akademikerbreen Group. These carbonates comprises the Grusdievbreen, Svanbergfjellet, Draken, and Backlundtoppen formations, all of which are conformable across the length of the outcrop belt (Fig. 2) and generally thin from south to north (Wilson, 1961), indicating that the cratonic margin lay north of the EGES basin (in present Svalbard coordinates) at the time of deposition. The Grusdievbreen Formation exceeds 600 m in thickness and is separated into two informal members (upper and lower) at one of only two major sequence boundaries in the Akademikerbreen Group. Whereas mid-shelf limestone rhythmites dominate the Grusdievbreen lithology, the overlying Svanbergfjellet contains abundant microbialaminites and stromatolites in additional to limestone ribbon rock. The Svanbergfjellet Formation is ~600 m thick in the south (Olav V Land), but thins dramatically to the north (Wilson, 1961). It is separated into four informal members (Wilson, 1961; Knoll and Swett, 1990), the lower two of which are separated by a second sequence boundary (Fig. 3). The ~200 m-thick Draken Formation consists predominantly of dolomitic intraformational conglomerates, microbialaminites, and grainstones deposited in a tidal flat/lagoonal setting

Fig. 2. Geological map of the north–south trending Neoproterozoic outcrop belt in northeastern Svalbard: Numbered boxes key stratigraphic sections measured and sampled for this study. Location names: 1) Svanbergfjellet, 2) Golitsynfjellet (north and south), 3) Dracoisen, 4) Raudberget, 5) Glintdalen, 6) Faksegåven, 7) Murchisonfjord. ESZ = Eolussletta Shear Zone; LFZ = Lomfjorden Fault Zone.

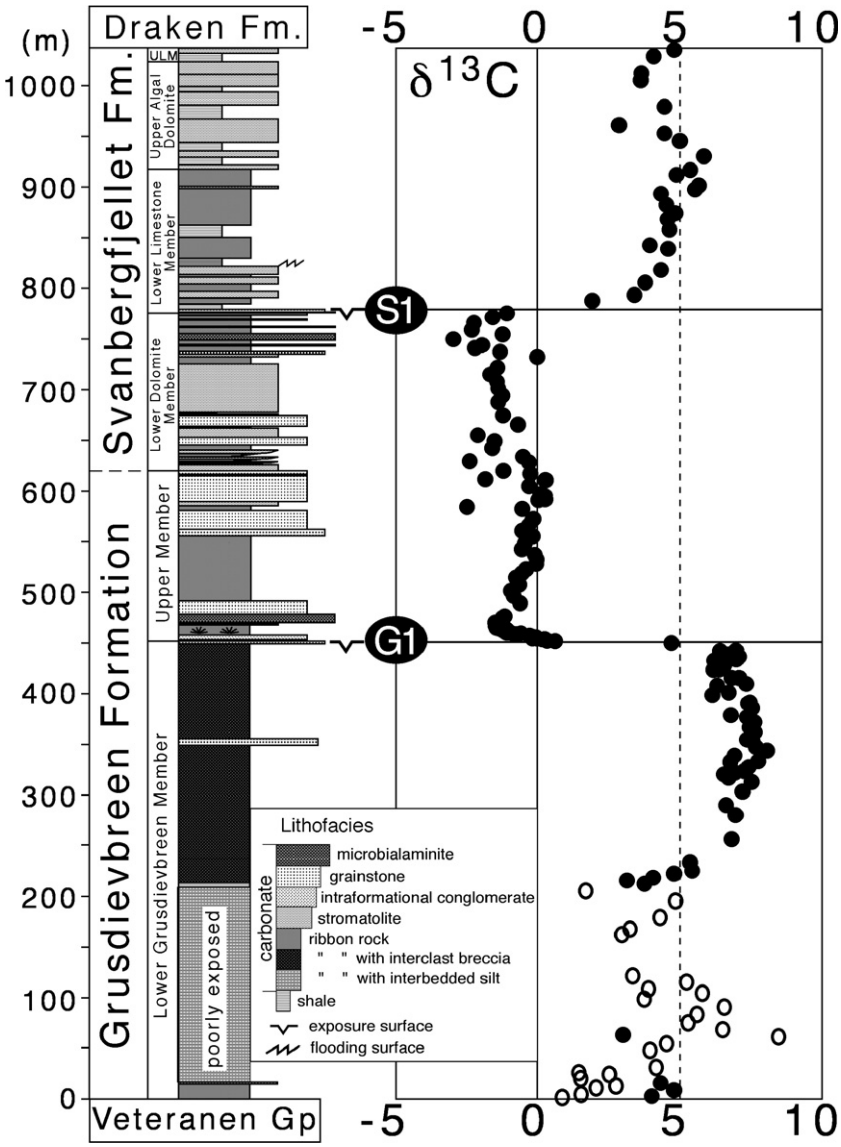


Fig. 3. Composite stratigraphic section and $\delta^{13}C$ data (closed circles) through the Grusdievbreen and Svanbergfjellet formations at measured section 7 (Murchisonfjord). Open circles are $\delta^{13}C$ data from measured section 6 to fill in limited data coverage through poorly exposed section at measured section 7.

(Knoll et al., 1991). The upper Draken Formation is gradational with the overlying Backlundtoppen Formation, which is ~500 m-thick and comprises black limestone ribbon rock, oolitic and pisolitic grainstone, and pale gray dolomite clastic grainstone and stromatolites (Wilson, 1961; Knoll et al., 1989). An influx of silt and fine sand into the EGES basin during deposition of the uppermost Akademikerbreen Group (Kinnvikka Member) marks the end of the long-lived carbonate platform (Fairchild and Hambrey, 1995; Halverson et al., 2004).

The overlying mixed carbonate-siliciclastic Polarisbreen Group contains two separate diamictites units. Halverson et al. (2004) interpreted these glacials as representing the beginning and end of a Marinoan snowball cycle (Fig. 1), and the lowermost Polarisbreen Group (Russøya Member of the Elbobreen Formation) as the chronostratigraphic equivalent of the Sturtian cap-carbonate sequence (Halverson et al., 2005). If this hypothesis is correct, it implies a minimum age of ~700 Ma for the top of the Akademikerbreen-Polarisbreen contact (cf. Brasier et al., 2000, though note the timing of the Sturtian glaciation in other successions remains poorly resolved). Alternatively, the glacigenic Petrovbreen Member (Fig. 1) may represent the Sturtian glaciation (e.g. Kennedy et al.,

Table 1
Isotopic and elemental data for 28 samples on which $^{87}Sr/^{86}Sr$ was determined from the Grusdievbreen and Svanbergfjellet formations

| Sample | Formation | Scaled stratigraphic height | $^{87}Sr/^{86}Sr$ | $\delta^{13}C$ | $\delta^{18}O$ | Mg/Ca (mol/mol) | Mn/Sr (mol/mol) | Mn (ppm) | Sr (ppm) |
|---|---|---|---|---|---|---|---|---|---|
| G341.464.5 | Svan. | 917.3 | *0.70659* | 4.88 | −6.32 | 0.799 | 1.598 | 105.8 | 105.6 |
| G341.445.3 | Svan. | 898.1 | 0.70661 | 4.34 | −6.08 | 0.016 | 0.046 | 29.6 | 1025.5 |
| G19.71.8 | Svan. | 851.8 | 0.70625 | 5.95 | −6.35 | 0.075 | 0.116 | 72.0 | 993.5 |
| G19.57.2 | Svan. | 843.5 | 0.70629 | 5.93 | −6.79 | 0.028 | 0.099 | 60.0 | 964.0 |
| G19.25.7 | Svan. | 805.7 | *0.70758* | 2.73 | −6.91 | 0.031 | 1.050 | 77.6 | 117.9 |
| G341.300 | Svan. | 752.8 | *0.70681* | −2.98 | −5.05 | 0.276 | 0.338 | 49.3 | 232.7 |
| G341.294.5 | Svan. | 747.3 | *0.70698* | −1.97 | −4.65 | 1.092 | 0.796 | 63.3 | 126.9 |
| G341.282.5 | Svan. | 735.3 | 0.70635 | −0.02 | −5.53 | 0.321 | 0.113 | 38.1 | 536.3 |
| G341.251.6 | Svan. | 704.4 | *0.70673* | −1.40 | −6.25 | 0.187 | 0.322 | 38.0 | 188.4 |
| G341.215.6 | Svan. | 668.4 | 0.70634 | −0.70 | −6.90 | 0.015 | 0.030 | 17.5 | 930.2 |
| G341.205.1 | Grus. | 657.9 | 0.70644 | −2.12 | −7.28 | 0.019 | 0.123 | 28.4 | 368.3 |
| G341.178 | Grus. | 630.8 | 0.70642 | −0.31 | −7.26 | 0.025 | 0.027 | 13.8 | 805.9 |
| M9.125.6 | Grus. | 617.3 | 0.70660 | 0.57 | −8.49 | 0.009 | 0.006 | 4.3 | 1241.8 |
| G341.146.6 | Grus. | 599.4 | 0.70637 | 0.08 | −6.92 | 0.034 | 0.020 | 18.4 | 1481.4 |
| M9.83.4 | Grus. | 575.1 | 0.70641 | −0.31 | −8.51 | 0.007 | 0.004 | 5.2 | 2029.7 |
| M9.55.0 | Grus. | 546.7 | 0.70640 | −0.75 | −9.17 | 0.015 | 0.002 | 2.8 | 2283.0 |
| G33.145.9 | Grus. | 488.9 | 0.70643 | −1.09 | −8.32 | 0.018 | 0.007 | 5.2 | 1236.9 |
| G148.158.7 | Grus. | 476.8 | 0.70635 | −1.25 | −8.14 | 0.017 | 0.029 | 12.5 | 695.9 |
| G33.131.7 | Grus. | 474.7 | 0.70644 | −1.01 | −8.33 | 0.018 | 0.041 | 13.7 | 594.1 |
| G148.149.2 | Grus. | 467.3 | 0.70640 | −1.46 | −8.40 | 0.024 | 0.121 | 45.4 | 271.3 |
| G148.140.3 | Grus. | 458.4 | *0.70699* | −0.22 | −9.85 | 0.010 | 0.677 | 40.9 | 96.3 |
| G33.112.1 | Grus. | 455.1 | *0.70884* | −0.44 | −11.75 | 0.020 | 1.249 | 104.7 | 133.7 |
| G148.136.3 | Grus. | 454.4 | 0.70624 | 0.33 | −8.85 | 0.011 | 0.16 | 28.6 | 281.8 |
| G148.126 | Grus. | 444.1 | 0.70625 | 6.42 | −7.01 | 0.024 | 0.012 | 13.2 | 1719.9 |
| G33.91 | Grus. | 434 | 0.70652 | 5.79 | −10.60 | 0.021 | 0.022 | 7.2 | 513.6 |
| G33.62.2 | Grus. | 405.2 | 0.70628 | 7.27 | −7.07 | 0.009 | 0.006 | 6.3 | 1692.4 |
| G33.14.5 | Grus. | 357.5 | 0.70626 | 6.55 | −6.26 | 0.026 | 0.006 | 9.7 | 2525.5 |
| G336.281.7 | Grus. | 281.7 | 0.70627 | 6.97 | −5.67 | 0.010 | 0.012 | 17.1 | 2278.5 |

Stratigraphic heights are all scaled to the composite section from measured section 7 (Fig. 3). $^{87}Sr/^{86}Sr$ data in italics are regarded as secondary based on Sr concentrations. See Supplementary materials for a complete tabulation of isotopic and elemental data.

1998), in which case the top of the Akademikerbreen Group is >700 Ma. An inferred cryptic unconformity beneath the Cambrian Tokammane Formation of the Oslobreen Group truncates the Polarisbreen Group (Knoll and Swett, 1987), and the absence of Ediacaran fossils beneath this contact (Knoll and Swett, 1987) suggests a minimum age of 575 Ma (Bowring et al., 2003) for the top of the Neoproterozoic succession in Svalbard (Fig. 1).

Previous studies revealed a series of $\delta^{13}C$ excursions in the Neoproterozoic succession of Svalbard (Knoll et al., 1986; Derry et al., 1992; Kaufman et al., 1997); negative $\delta^{13}C$ anomalies in the Polarisbreen Group are clearly associated with glacial episodes (Knoll et al., 1986; Fairchild and Spiro, 1987; Fairchild et al., 1989; Kaufman et al., 1997; Halverson et al., 2004). Carbonates in the Akademikerbreen Group were shown to be generally very $^{13}C$-enriched, with the exception of negative $\delta^{13}C$ values in the upper Grusdievbreen and lower Svanbergfjellet formations (Knoll et al., 1986; Kaufman et al., 1997), which are the focus of this paper.

## 3. Materials and methods

### 3.1. Sample collection and preparation

All samples used in this study were collected in the course of measuring stratigraphic sections. Samples were chosen so as to minimize veining, fractures, and weathered surfaces. All samples were slabbed, polished and subsampled with 1–5 mm dental drill bits. Splits of sample powder were used for all geochemical analyses described below.

### 3.2. Stable Isotopes

$\delta^{13}C$ and $\delta^{18}O$ isotope data (VPDB) were acquired on a VG Optima dual inlet mass spectrometer attached to a VG Isocarb preparation device in the Harvard University Laboratory for Geochemical Oceanography. External error ($1\sigma$) better than ±0.1‰ was achieved for both $\delta^{13}C$ and $\delta^{18}O$. See Halverson et al. (2004) for a description of methods. See Supplementary materials for tabulated data.

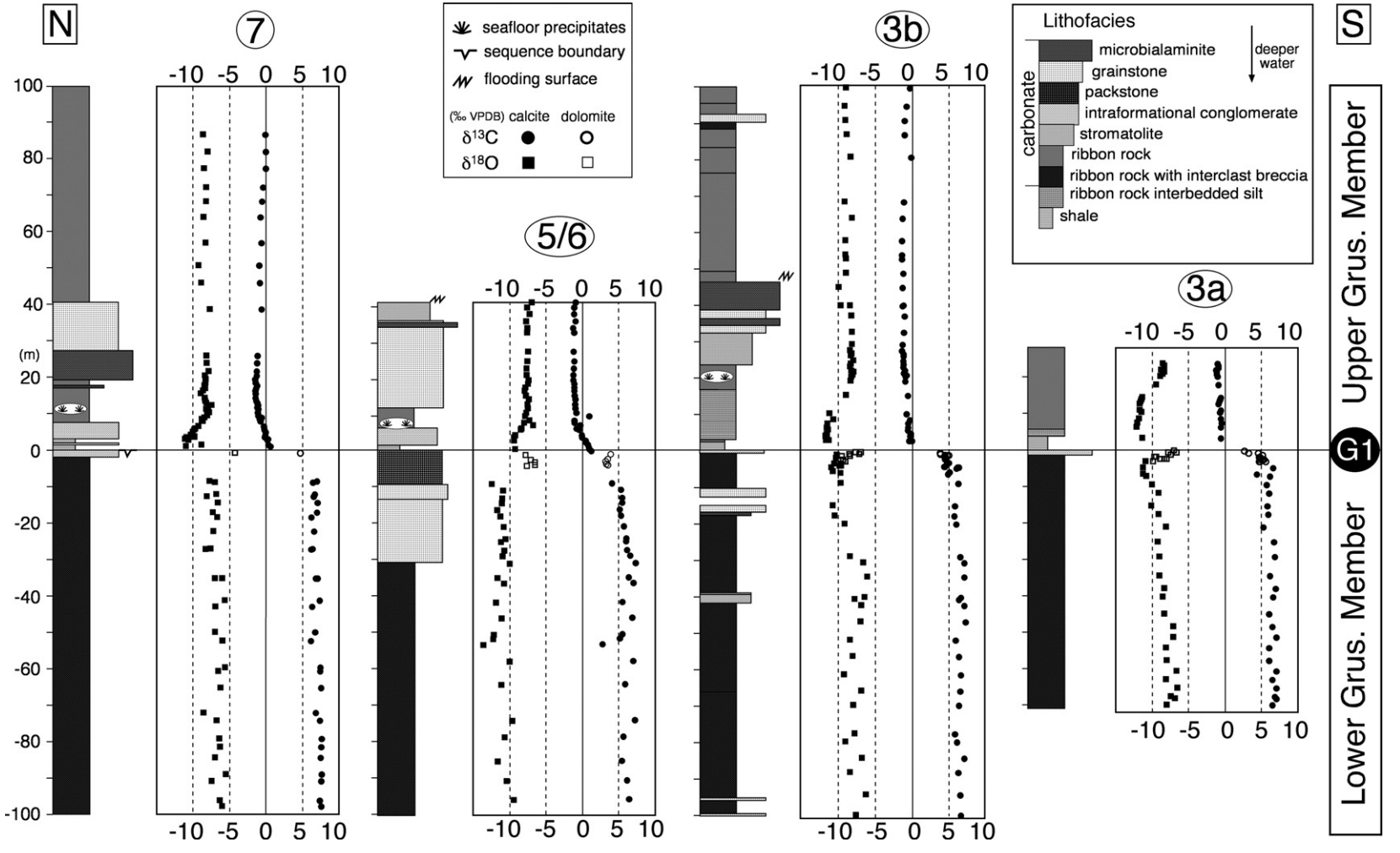


Fig. 4. Stratigraphic, $\delta^{18}O$, and $\delta^{13}C$ profiles spanning the G1 sequence boundary in the Grusdievbreen Formation in multiple sections. The 0-m datum is the G1 sequence boundary, which is easily identified in section along the length of the outcrop belt (Fig. 5a). The second column from the left is a composite, with the upper Grusdievbreen Formation derived from measured section 5, and the lower Grusdievbreen Formation from measured section 6.

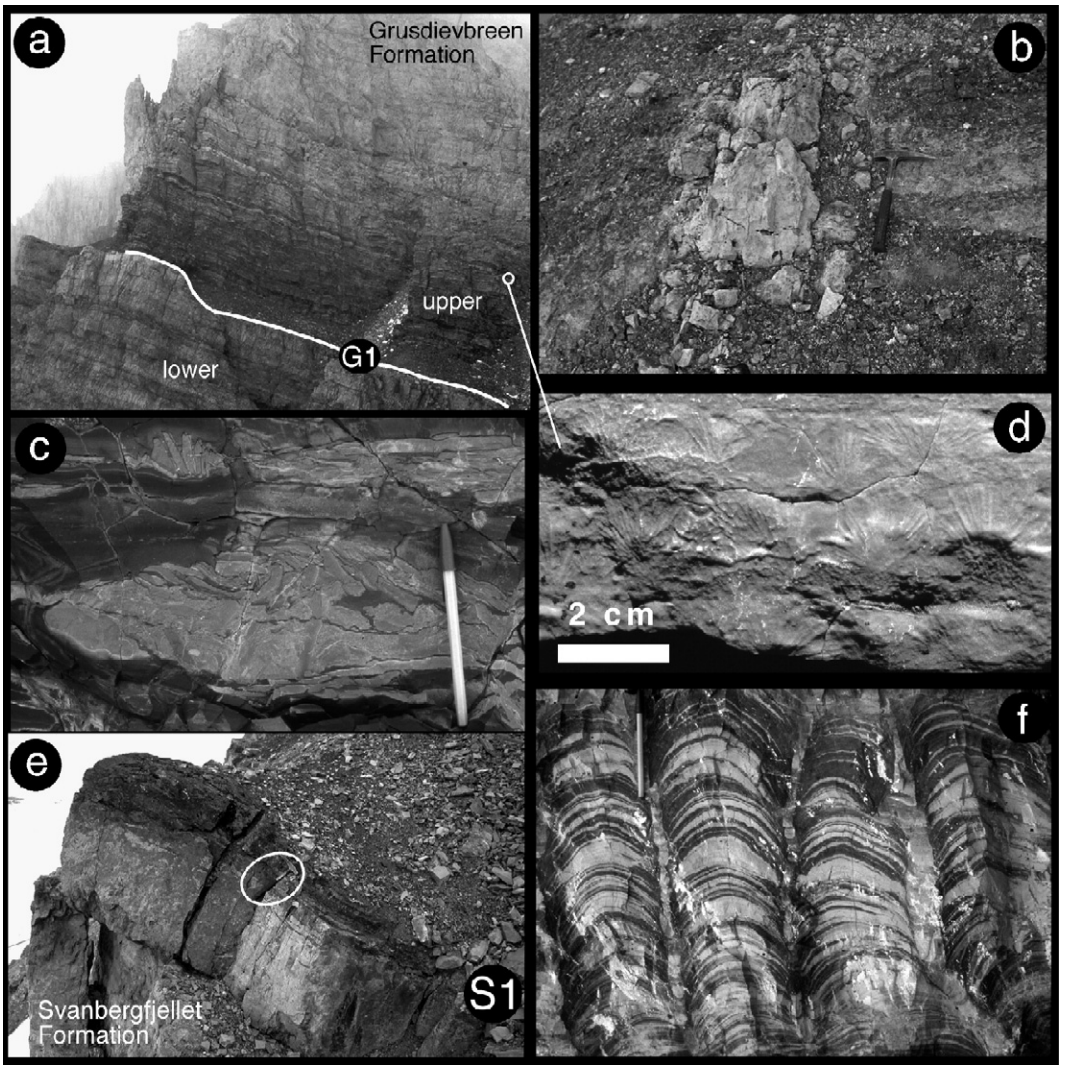


Fig. 5. Field photographs of the Grusdievbreen and Svanbergfjellet formations. a) G1 sequence boundary (white line) separating the upper and lower members of the Grusdievbreen Formation at measured section 3b. Note the relief on this contact (2 m), and the sharp change in lithology in the parasequence above the boundary. b) Karst pipe consisting of heavily recrystallized dolomite packstone penetrating limestone grainstone ~10 m beneath the G1 contact at measured section 6. c) Edgewise limestone breccias within the silty member above the G1 sequence boundary. Note the breccia bundles are continuous with coherent layers from which the clasts are derived. d) Aragonite pseudomorphs ("crystal fans") forming a continuous seafloor cement in limestone ~20 m above the G1 boundary at measured section 5. The crystal fans occur along bedding surfaces and the space between them is filled by onlapping micrite, indicating that they are primary depositional features. e) The S1 sequence boundary at measured section 1 (the type section of the Svanbergfjellet Formation). The hammer, for scale (outline in white circle), is lying on the brecciated, silicified, and ferruginized zone beneath black shales of the Middle Limestone Member. Despite heavy brecciation and silicification of the exposure surface, no evidence of erosional relief is apparent on outcrop scale. f) Columnar *Minjaria* stromatolites in the Lower Limestone Member form a distinctive biostrome 10–15 m above the S1 boundary throughout northeast Svalbard (Knoll and Swett, 1990). The hammer and pen (for scale in b, c, e, and f) are 13 cm and 33 cm long, respectively.

### 3.3. Elemental chemistry

Elemental analyses (Ca, Mg, Sr, Mn, Fe) were performed on a Jovin Yvon 46P ICP-AES mass spectrometer in the Harvard University Laboratory for Geochemical Oceanography. All samples were prepared by dissolving ~4 mg of carbonate powder in ~4 ml of 2% nitric acid. SCP multielement and single element standards were used for element-specific calibration at the beginning of each run. External error ($1\sigma$), determined by repeat analyses, was <7% for all elements, with the best precision achieved for Ca, Mg, and Sr.

### 3.4. Strontium isotopes

New $^{87}Sr/^{86}Sr$ data presented in Table 1 were acquired at the MIT Radiogenic Isotope Laboratory. 5–10 mg aliquots of powdered carbonate were leached sequentially 3–5 times for 15–45 min in 0.2 M ammonium acetate to remove loosely bound Sr cations (cf. Bailey et al., 2000). Carbonate was dissolved in 0.5 N acetic acid and insoluble residue was removed by centrifuging. Sr was isolated via standard column chemistry techniques and analyzed on a VG Sector 54 (TIMS). All samples are referred to a standard value of 0.710250 for NBS 987, whose long-term average value on the Sector 54 is 7.10246, with 2-$\sigma$ internal precision of 0.000016.

## 4. Stratigraphy and geochemistry of the lower Akademikerbreen Group

### 4.1. Grusdievbreen Formation

The lower Akademikerbreen Group is well exposed at measured sections 4, 5, 6, and 7. Fig. 3 presents a composite section from measured section 7 (Murchisonfjord), where we have the most detailed stratigraphic and isotopic coverage. We use this section as a reference for discussion of the stratigraphy and carbon isotope record through the Grusdievbreen and Svanbergfjellet formations.

The Grusdievbreen Formation is ~600 m thick, relatively uniform across the length of the outcrop belt, transitional with the underlying Veteranen Group (Wilson, 1961), and informally separated here into an upper and lower member (Fig. 3). The base of the Grusdievbreen Formation is identified by the first dolomite-rich beds above finely laminated, hummocky cross stratified siltstones of the Oxfordbreen Formation (Wilson, 1961). The lower part of the Lower Grusdievbreen Member consists of intercalated siltstone, nodular (dolomite and limestone) rhythmites ribbon rock (Knoll and Swett, 1990), and minor isolated stromatolite mounds. Sampling through this interval is sparse due to the abundance of silt and poor exposure in some sections, but available data indicate $\delta^{13}C$ values near 1‰ at the base of the Grusdievbreen Formation and variable and more $^{13}C$-enriched values through the succeeding 200 m (Fig. 3).

A colorful 10 m-thick unit of orange and pink-weathering intraformational breccia with interbedded green and red shale overlies a flooding surface in the middle of the Lower Grusdievbreen Member and coincides with a spike to $\delta^{13}C$ values as low as 1.7‰ (Fig. 3). $\delta^{13}C$ values rise gradually and smoothly up to 8‰ through ~50 m of strata above the flooding surface, then remain high through most of the remaining 200+ m of the Lower Grusdievbreen Member, which consists almost exclusively of monotonous mid-shelf black limestone ribbon rock (Knoll and Swett, 1990) with interbedded storm-generated intraclast breccias and minor grainstone. $\delta^{13}C$ values begin to decline just below a prominent sequence boundary (G1) that separates the upper and lower members at ~450 m above the base of the Grusdievbreen Formation (Fig. 1).

The G1 sequence boundary and bracketing stratigraphy, discussed in more detail below, coincide with a sharp decline in $\delta^{13}C$ (Fig. 4). The lower 20 to 40 m above the G1 boundary comprise a brick-red, upward-shoaling parasequence that stands out amidst the background stratigraphy (Fig. 5). $\delta^{13}C$ values remain low (<0.5‰) through the remainder of the Grusdievbreen Formation. Limestone ribbon rock and clastic grainstones dominate the lithology of the Upper Grusdievbreen Member, but stromatolite bioherms are also locally abundant. Molar tooth structures are common in the ribbon facies and molar tooth breccias form the base of some ribbon rock beds. Styolites are common throughout the Upper Grusdievbreen Member and demonstrate significant compaction of the sediment column.

#### 4.1.1. The G1 boundary

The G1 sequence boundary is best exposed on the eastern side of the Golitsynfjellet nunatak, alongside the Akademikerbreen Glacier in Olav V Land (Fig. 2), where two sections (3a,b) 2 km apart have been measured (Fig. 5a). There, the uppermost 1.3 m beneath the G1 sequence boundary is a coarse, dolomitic intraformational conglomerate. Erosional relief developed on the exposure surface is visible on the outcrop and cuts down as much as 2 m, in places removing the dolomitic conglomerate bed (Fig. 5a) and demonstrating that at least one phase of dolomitization preceded erosional truncation. To the north, in the Lomfjord region (Fig. 2, measured sections 5 and 6), a heavily recrystallized, yellow, vuggy dolomitic packstone directly underlies the G1 boundary, forms a bed up to 4 m thick, and fills karst pipes that developed in the underlying limestones. At measured section 6, the karst is pervasive just below the boundary and individual pipes in contact with the exposure surface extend as much as 10 m deep. Grikes up to 0.5 m wide are developed along joints and occur as much as 20 m below the G1 surface (Fig. 5b). Since dolomitization of the packstone must have occurred after the development of G1 exposure surface in this region, it appears that dolomitization of the Akademikerbreen platform was ongoing spanning the sequence boundary. No evidence of karstification or erosion related to the G1 sequence boundary has been identified around Murchisonfjord,

although it should be noted that this surface is not well exposed in this region.

At Golitsynfjellet, a bed of green silt overlies the sequence boundary and varies in thickness up to 2 m, filling erosional relief on the G1 sequence boundary. The green silt passes transitionally into red silt, which is generally finer grained but contains coarse-grained lenses and scattered carbonate intraclasts. Scour surfaces and hummocky cross stratification are common in the red silt facies. The first coherent carbonate lenses appear at 3.8 m above the boundary. These white to pink limestone lenses alternate with silt layers, vary in thickness from 1 to 6 cm, are discontinuous, and are intermittently brecciated, suggesting early lithification on the seafloor. Large tabular clasts from these beds are commonly bundled edgewise in packages filling pockets scoured into underlying silt layers and draped by red silt (Fig. 5c). In places, these clasts are imbricated, whereas others bundles resemble "beach rosettes," (Fig. 5c) suggesting deposition under oscillatory flow. Whereas edgewise conglomerates are often associated with shallow-water conditions, such as a beaches or tidal flats (Demicco and Hardie, 1994, p. 42), the association of the breccias above the G1 boundary with hummocky cross stratification suggests the lowermost carbonate beds were deposited between fair weather and storm weather wave base and that storm waves may have caused the disaggregation of the carbonate lenses.

Up section, the percentage of silt gradually decreases and discrete silt layers disappear by ~20 m above the exposure surface. At the same level, crystal fan pseudomorphs up to ~3 cm in diameter occur within a 1 m-thick horizon. Individual crystals have square terminations, indicating that the fans were originally aragonitic. The crystal fan horizon is best developed at measured section 5, where the fans are tightly packed in continuous layers (Fig. 5d) and account for >25% of total sediment volume. The crystal fan layers are infilled and draped by micrite, indicating that they grew directly on the seafloor, analogous to seafloor cements in some Marinoan cap–carbonate sequences (Hoffman and Schrag, 2002).

Above the crystal fan horizon, recrystallized, chalky limestone ribbon rock passes upward into small (2–4 cm diameter), columnar stromatolites, grainstones and microbialaminites, up to a flooding surface that marks the top of the basal parasequence of the upper member of the Grusdievbreen Formation (Fig. 4). At measured section 2, the parasequence is 47 m thick, whereas in Murchisonfjord (measured section 7), it is only half as thick. This difference in thickness is controlled, at least partly, by the abundance of siliciclastic sediment in the parasequence, which increases from north to south. This pattern of southward thickening is at odds with the hypothesis that the paleo-cratonic margin lies northward of the Svalbard outcrop belt and suggests either that the Murchisonfjord region was a zone of sediments bypass or that another siliciclastic sediment source existed to the south or southwest. Despite the differences in thickness, the parasequence above the G1 everywhere stands out starkly against the background stratigraphy of predominantly black limestone ribbon rock (Fig. 5a).

In all measured sections (Fig. 4), the $\delta^{13}C$ trend is identical across the G1 boundary, beginning to decline from a high of 7‰ directly beneath the exposure surface, then dropping sharply across the boundary, and gradually declining to a low of ~−1.5‰ roughly coincident with the crystal fan horizon (Fig. 4). However, whereas $\delta^{13}C$ values in the lowermost limestone above the boundary in our two Golitsynfjellet sections (3a,b) are already negative in the northern two sections, $\delta^{13}C$ values are slightly positive directly above the sequence boundary and gradually decline to <0‰ over the next 5 m. Allowing for differences in sedimentation rates, the $\delta^{13}C$ values across the G1 boundary in all sections are otherwise identical within 0.5‰ (Fig. 4). Therefore, the northern sections appear to preserve a more complete record of the evolution of marine $\delta^{13}C$ values spanning the sequence boundary, perhaps because the first carbonates to precipitate were not as diluted by incoming silt.

Just as the $\delta^{13}C$ trends in all sections are virtually identical across the G1 boundary, so also are the patterns in $\delta^{18}O$ values reproduced in multiple sections (Fig. 4). Beneath the exposure surface, $\delta^{18}O$ values rise abruptly from ~−11 to −6‰. In the lowest limestones above the surface, $\delta^{18}O$ values are −9 to −12‰. $\delta^{18}O$ values then rise gradually over the next10 to 20 m of section to an average of −8‰ (Fig. 4), which is a typical value for limestones in the Akademikerbreen Group (Derry et al., 1992; Halverson, 2003). The perturbation in the unusually smooth and reproducible $\delta^{18}O$ trend is clearly related to the G1 sequence boundary, but does it represent a primary seawater signal?

The concentration of dolomite beds in the Grusdievbreen Formation at the G1 boundary suggests that dolomitization was related to the sea level fall that exposed the Akademikerbreen platform. Variable truncation of the dolomite unit at measured sections 2a,b indicates that one phase of dolomitization must have preceded development of the G1 sequence boundary. On the other hand, at measured section 6, dolomitized packstone fills karstic cavities, indicating that dolomitization also proceeded after the platform had been subaerially exposed. Therefore, the similar increase in $\delta^{18}O$ values beneath the exposure surface in both regions, despite the apparent difference in timing of

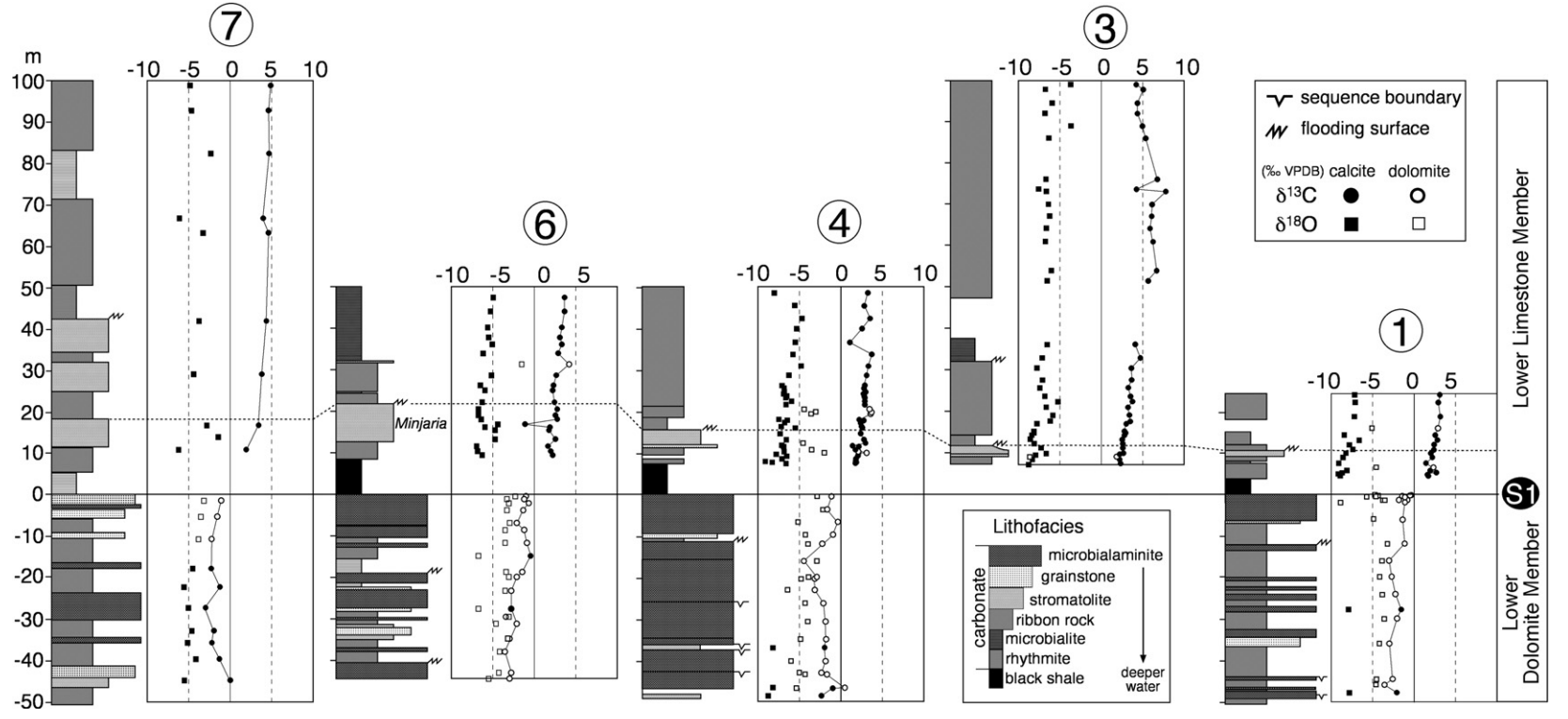


Fig. 6. Stratigraphic, $\delta^{18}O$, and $\delta^{13}C$ profiles spanning the S1 sequence boundary in the Svanbergfjellet Formation from 5 measured sections. The 0-m datum is the S1 sequence boundary, which is everywhere brecciated and silicified (Fig. 5e). Dashed line above the S1 boundary shows correlation of the flooding surface at the top of the *Minjaria* biostrome.

dolomitization, suggests that the positive upward trend in $\delta^{18}O$ values records a secondary rather than primary seawater signal. A cross-plot of $\delta^{18}O$ vs. Mg/Ca for all samples spanning the sequence boundary shows a clear positive, linear trend, the least-squares best fit of which is the line $\delta^{18}O = 3.77(Mg/Ca) - 10.3‰$ (Fig. 7). The 3.77‰ difference between stoichiometric calcite (Mg/Ca ≈ 0) and dolomite (Mg/Ca ≈ 1) is consistent with the estimated equilibrium fractionation between these two carbonate phases (Land, 1980; Kah, 2000) and suggests that the positive deflection in $\delta^{18}O$ is purely an equilibrium isotope effect, with the most $^{18}O$-enriched values corresponding to most heavily dolomitized samples.

The *y*-intercept (Mg/Ca = 0) of the Lower Grusdievbreen Member (LGM) dolomitization trend (−10.3‰) is significantly lower than average $\delta^{18}O$ values in the Akademikerbreen Group but is only slightly more negative than the average $\delta^{18}O$ composition (−9.6‰) of the best-preserved limestones (Mg/Ca, Mn/Sr < 0.1) in the 20 m beneath the G1 boundary (Fig. 8). In contrast, the average $\delta^{18}O$ value in the best-preserved limestones from 20 to 120 m beneath the G1 boundary is −7.4‰ (Fig. 8). Therefore, rather than a trend of increasing $\delta^{18}O$ directly below the G1 boundary, as seen in the bulk data (Fig. 4), $\delta^{18}O$ data from the best preserved samples reveal a more gradual decline of ~2‰ that begins before the downward shift in $\delta^{13}C$ values (Fig. 8).

In all measured sections $\delta^{18}O$ values directly above the sequence boundary are deflected negative of the background trend (Fig. 4). A combination of field observations and geochemical data suggest that meteoric diagenesis contributed to this signal. Firstly, the limestones in the lower 30 m above the G1 boundary are generally recrystallized, and despite evidence for primary aragonite precipitation, have an average Sr concentration of ~150 ppm, compared to >1000 ppm in limestones well below and above the boundary. Based on the predominance of red silt in this stratigraphic interval, the diagenetic fluids were oxidizing. A cross-plot of Sr and Mn concentrations in Fig. 7b shows a distinct dog-leg trend with [Sr] decreasing precipitously with increasing [Mn] in samples with [Mn] < 50 ppm, before flatting out in samples with [Mn] > 50 ppm. This trend is characteristic of carbonate systems that have experienced a variable degree of fluid–rock interaction during meteoric diagenesis (Brand and Veizer, 1980, 1981; Banner and Hanson, 1990; Jacobsen and Kaufman, 1999). This diagenesis also affected the oxygen isotopic composition of limestones above the G1 boundary as seen in the $\delta^{18}O$–Mn/Sr cross-plot in Fig. 7c. Whereas significant variation in $\delta^{18}O$ occurs independent of changes in Mn/Sr, samples from the lower part of the Upper Grusdievbreen Member (UGM) plot along a logarithmically decreasing trend (Fig. 7c inset) as predicted by models of meteoric diagenesis (Banner and Hanson, 1990; Jacobsen and Kaufman, 1999).

Considering this evidence for alteration by meteoric waters, it is not surprising that the $\delta^{18}O$ anomaly above the G1 boundary (Fig. 4) is absent in a plot of $\delta^{18}O$ data from only the best-preserved limestones (Fig. 8). Therefore, despite the reproducibility of the low-$\delta^{18}O$ trend above the G1 boundary in all sections (Fig. 4), it is regarded as purely a secondary alteration signature. In contrast, $\delta^{13}C$ in the same samples appears insensitive to variation in Mn/Sr (Fig. 7d), suggesting the smoothly declining $\delta^{13}C$ trend (Fig. 8) is a primary seawater signal.

### 4.2. The Svanbergfjellet Formation

The Svanbergfjellet Formation, which is well exposed in all sections except measured section 4 (Figs. 2, 6), is informally divided into four members (Knoll and Swett, 1990), and thins dramatically from over ~600 m thick in southern exposures to ~100 m in the northernmost exposure (Wilson, 1961), suggesting a northward cratonic margin to the EGES basin at this time (Halverson et al., 2005). The contact with the Grusdievbreen Formation is poorly defined and difficult to pinpoint in the field, but is generally identified by a switch from limestone to dolomite and concomitant increase in closely spaced flooding surfaces and abundant shallower-water facies. The Lower Dolomite Member (Fig. 3) is distinguished by the concentration of faults and folds in this unit, presumably due to the more brittle behavior of the dolomite than surrounding limestone units during Caledonian shortening.

Microbialaminites and small, laterally-linked stromatolites are particularly common facies in the Lower Dolomite Member (Fig. 3). In contrast, in the Upper Algal Dolomite Member (Fig. 3), larger stromatolites comprising discrete biostromes (Knoll and Swett, 1990) are more common and variably include *Baicalia*, *Colonella*, *Tungusia*, and *Conophyton*. The Lower and Upper Limestone members consist predominantly of black, ribbony, and often hummocky cross-stratified limestone with abundant molar tooth structures. However, stromatolites also occur in the Lower Limestone Member and include a prominent *Minjaria* bed (Figs. 5, 6) that makes a useful stratigraphic marker across the outcrop belt (Knoll and Swett, 1990). All four members of the Svanbergfjellet Formation thin to the north, although some of the variability between sections may be attributable to tectonic thickening.

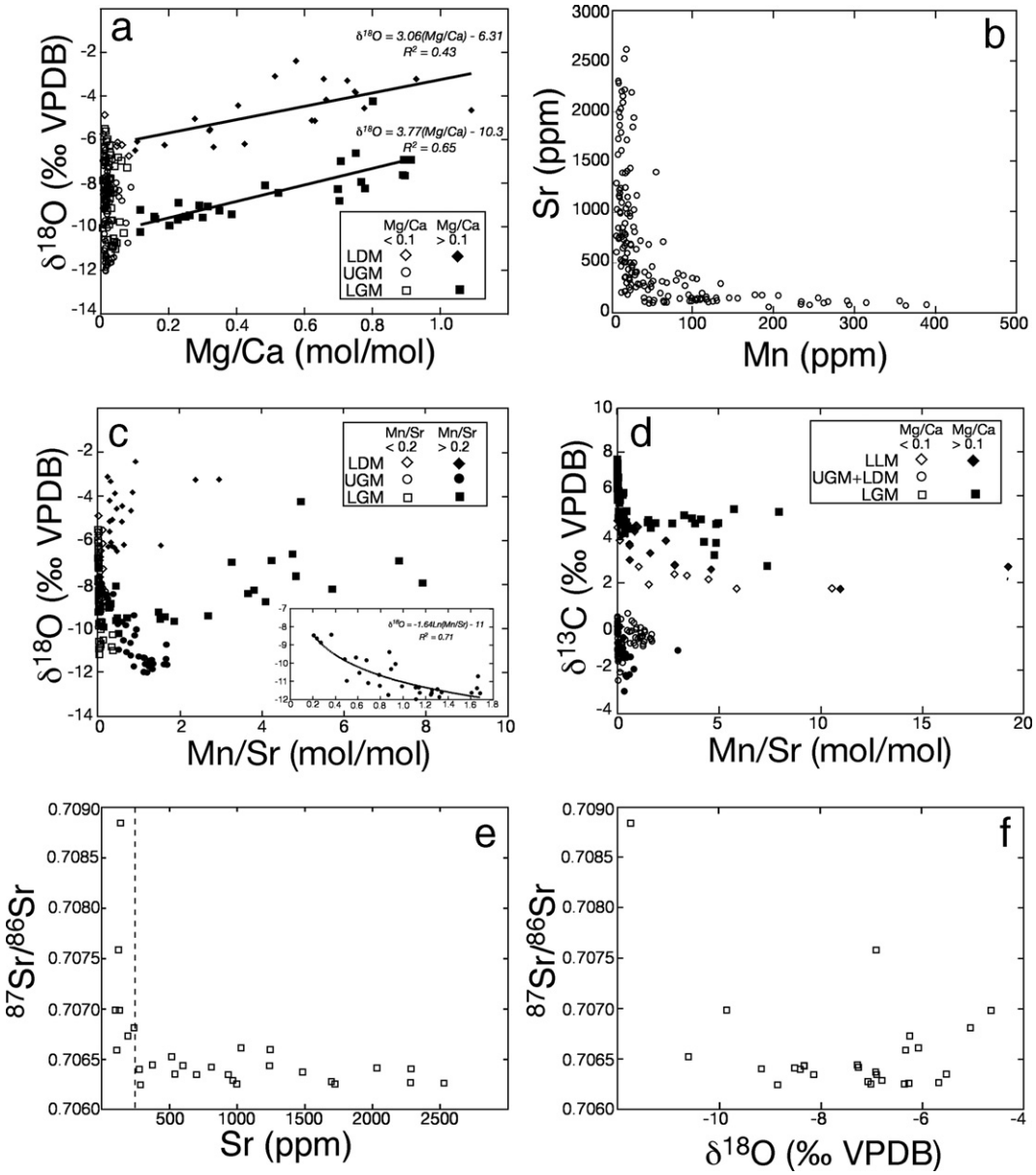


Fig. 7. Isotopic and elemental data from the Grusdievbreen and Svanbergfjellet formations. a) $\delta^{18}O$–Mg/Ca cross-plot shows two distinct dolomitization trends whose slopes are consistent with the approximate equilibrium isotope fractionation between dolomite and calcite (e.g. Land, 1980). The upper trend is from dolomites in the Lower Dolomite Member (LDM) of the Svanbergfjellet Formation, and the lower trend is from the Lower Grusdievbreen Member (LGM). The LDM trend is about 4‰ heavier than the LGM trend, implying a higher initial $\delta^{18}O$ composition in the former and consistent with data from the best preserved limestones that show higher $\delta^{18}O$ values beneath the S1 boundary than beneath the G1 boundary (Fig. 8). b) Sr–Mn concentration cross-plot shows a typical pattern for meteoric diagenesis of originally aragonitic limestones (e.g. Banner and Hanson, 1990). c) $\delta^{18}O$–Mn/Sr cross-plot shows significant variability, but three distinct patterns are visible. An inferred meteoric diagenesis trend of logarithmically decreasing $\delta^{18}O$ with increasing Mn/Sr (inset) in limestones from the lower part of the Upper Grusdievbreen Member (UGM), high Mn/Sr values (>2) corresponding to dolomitized samples in the LDM and upper UGM, and a wide range (6‰) in $\delta^{18}O$ independent of Mn/Sr. d) $\delta^{13}C$–Mn/Sr cross-plot shows a distinct diagenetic trend of decreasing $\delta^{13}C$ with increasing Mn/Sr in both dolomite and limestone samples in the lower part of the Lower Limestone Member (LLM), which suggests that primary $\delta^{13}C$ values should be slightly heavier (1 to 2‰) in these samples. e) $^{87}Sr/^{86}Sr$–Sr cross-plot shows a typical diagenetic pattern in which $^{87}Sr/^{86}Sr$ is nearly invariant in samples with Sr concentrations >250 ppm (dashed line), but sharply rising $^{87}Sr/^{86}Sr$ in samples with Sr <250 ppm. Therefore, only samples with >250 ppm Sr are regarded as primary. f) $^{87}Sr/^{86}Sr$–$\delta^{18}O$ cross-plot shows no systematic variation in Sr isotope ratios in samples with $\delta^{18}O > -9‰$.

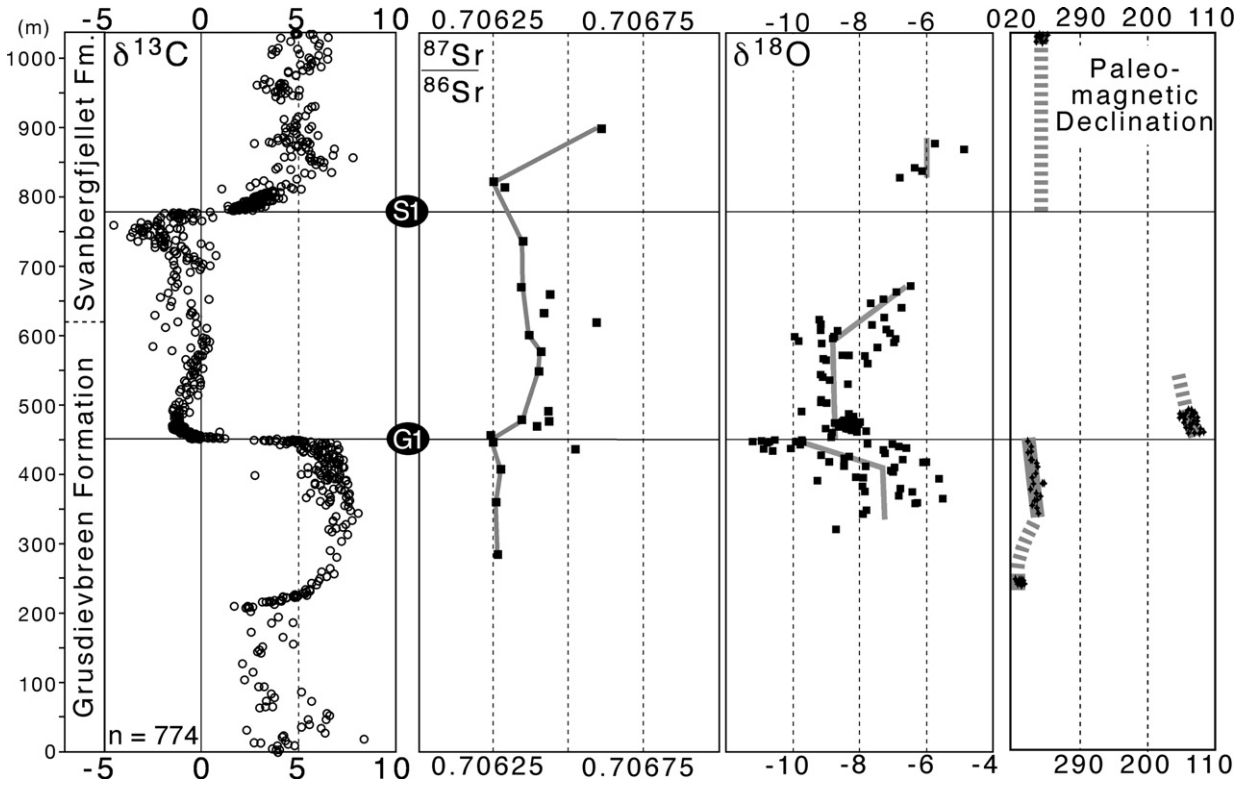


Fig. 8. Composite isotopic and paleomagnetic records through the Grusdievbreen and Svanbergfjellet formations (data in Supplementary materials). The $\delta^{13}C$ record represents all data from all measured and sampled sections. $^{87}Sr/^{86}Sr$ data are from samples with [Sr] > 250 ppm in measured sections 3, 4, and 7. Grey line represents the best approximation of seawater $^{87}Sr/^{86}Sr$ spanning the Bitter Springs isotope stage. $\delta^{18}O$ is from all measured sections with elemental data for which Mg/Ca and Mn/Sr < 0.1. The paucity of data spanning the S1 boundary reflects the preponderance of dolomite in this stratigraphic interval, whereas the lack of data in the upper Svanbergfjellet Formation is the artifact of the absence of elemental data for samples from this interval. The right-hand column is a composite plot of paleomagnetic data from the Grusdievbreen and Svanbergfjellet formations, summarized from Maloof et al. (2006) and demonstrating an ~55° discordance in paleodeclination across the G1 boundary and a return to pre-G1 paleodeclination in the Svanbergfjellet Formation. All opposite polarity intervals are reversed for simplicity, and inclination data is omitted as it varies little through the plotted interval.

Just as the G1 sequence boundary in the Grusdievbreen Formation delineates the sharp decline in $\delta^{13}C$ values at the onset of the low $\delta^{13}C$ interval in the lower Akademikerbreen Group, a second sequence boundary (S1) at the contact between the Lower Dolomite Member and Lower Limestone Member marks the abrupt return to positive $\delta^{13}C$ values in the Svanbergfjellet Formation (Figs. 3, 6). Following the return to $^{13}C$-enriched values in the Lower Limestone Member, $\delta^{13}C$ values vary around a mean of 5‰ with a pair of discernible fluctuations of 3–4‰ in amplitude that do not correspond to any perceptible change in sedimentation (Fig. 3). Spitsbergen sections are slightly $^{13}C$-enriched (0–1.5‰) relative to Nordaustlandet, but otherwise, the isotopic trend is virtually identical in the two regions (Fig. 6).

### 4.2.1. The S1 boundary

The S1 sequence boundary in the lower Svanbergfjellet Formation separates dominantly shallow-water, cyclic dolomites of the Lower Dolomite Member (LDM) below from deeper-water sediments of the Lower Limestone Member (LLM) above. This sequence boundary occurs along the length of the outcrop belt, but like the G1 boundary, is better developed in Ny Friesland, where the uppermost 0.5 m of the Lower Dolomite Member is typically heavily silicified and brecciated (Fig. 5e) and sharply overlain by 5 to 8 m of black shale (green shale in Nordaustlandet). The boundary is also ferruginized in most sections, but this iron enrichment could have been a secondary effect related to leaching from the overlying black shales. No erosional relief is apparent on outcrop scale, and the cyclic pattern of the underlying stratigraphy precludes determining the extent, if any, of regional scale truncation.

The black shales comprise the base of an upward-shoaling parasequence and grade upward into hummocky cross-stratified and marly dolomite ribbon rock. This storm-dominated facies passes transitionally into a regionally extensive biostrome, which consists of the

stromatolite *Minjaria* (Fig. 5f) in most locations, but also contains *Conophyton* near the top of the bed in the Lomfjord region and Nordaustlandet. The top of the biostrome is a flooding surface and in all measured Spitsbergen sections is overlain by a thick stack (>100 m) of bituminous rhythmites and ribbon rocks of the Lower Limestone Member. In some sections, the rhythmites contain crinkly laminae, presumably the remnants of microbial mats growing on the seafloor beneath storm wave base. In Nordaustlandet, intermittent stromatolites persist above the *Minjaria* biostrome and may be correlative with the microbially-influenced sediments in Spitsbergen sections.

$\delta^{13}C$ values in the upper part of the Lower Dolomite Member vary from 0 to −5‰ in both limestone and dolomite samples, but generally hover near −3‰ and show a slight rise beneath the S1 boundary. $\delta^{13}C \approx 2‰$ in the lowermost carbonates above the sequence boundary, and continues to rise gradually upsection to 5 to 7‰, typical values for the upper Svanbergfjellet Formation. This trajectory of rising $\delta^{13}C$ in the lower part of the Lower Limestone Member (Figs. 6, 8) is reproduced in detail in all sections, and analagous to the negative $\delta^{13}C$ shift at the G1 sequence boundary, this trend is clearly associated with the S1 sequence boundary. However, $\delta^{13}C$ values in the both dolomite and limestone samples in the lower part of the Lower Limestone Member show a distinct, logarithmically decreasing trend with increasing Mn/Sr ratios (Fig. 7d). This decrease in $\delta^{13}C$ with inferred increase in the extent of fluid–rock interaction may be in part related to mobilization and oxidation of organic matter from the black shales at the base of the Lower Limestone Member. In any case, this pattern suggests that the preserved $\delta^{13}C$ values in the lower part of the Lower Limestone Member may have been depleted in $^{13}C$ by as much as 2‰ during diagenesis. However, even if these samples were disregarded, the S1 sequence boundary would still delineate a sharp rise in $\delta^{13}C$ values.

The $\delta^{18}O$ composition of carbonates bracketing the S1 boundary is heavily influenced by the abundance of dolomite in the lower Svanbergfjellet Formation. Like the dolomitized samples beneath the G1 boundary, these Svanbergfjellet dolomites define a coherent swath in a cross-plot of $\delta^{18}O$ versus Mg/Ca (Fig. 7a). The best fit to these data is the line $\delta^{18}O = 3.06(Mg/Ca) - 6.31$. This dolomitization trend is offset 4‰ higher than the trend through the Grusdievbreen dolomites. Similarly, the $\delta^{18}O$ composition of the best-preserved limestones in the Svanbergfjellet Formation is on average heavier than that in the Lower Grusdievbreen Member (Fig. 8). If this difference reflects the primary depositional environment, then either the waters of the EGES basin were more restricted and saline or significantly cooler prior to the S1 positive $\delta^{13}C$ shift than before the G1 negative shift. The Svanbergfjellet dolomitization trend shows more scatter than the Grusdievbreen trend (Fig. 7a), but this could be due to the fact that the dolomite in the Lower Dolomite Member spans ~150 m, and the original $\delta^{18}O$ of carbonates deposited in this interval may have varied.

### 4.3. Strontium isotopes

We have analyzed 28 carbonate samples spanning the G1 and S1 boundaries for $^{87}Sr/^{86}Sr$ (Table 1). The density of data is greatest in the Grusdievbreen Formation, where limestones are very pure and have Sr concentrations of 1000–3000 ppm. The Sr concentration of ancient carbonates is very sensitive to the degree of fluid–rock interaction experienced during meteoric diagenesis (Brand and Veizer, 1980) and declines sharply with increasing Mn concentration (Fig. 7b). Although meteoric waters have low Sr concentrations, they are highly radiogenic, such that during meteoric diagenesis, the $^{87}Sr/^{86}Sr$ ratio of carbonates increases. This effect is negligible where the fluid–rock interaction is minimal and Sr concentrations remain high, but becomes very large where Sr concentrations are low (Banner and Hanson, 1990; Jacobsen and Kaufman, 1999). A cross-plot of $^{87}Sr/^{86}Sr$ versus Sr concentration (Fig. 7e) clearly shows this pattern, with a very steep radiogenic trend occurring in samples with [Sr]<250 ppm. On the other hand, data from samples with [Sr]>250 ppm define a flat, linear trend, showing no systematic increase in $^{87}Sr/^{86}Sr$ with decreasing Sr concentration. No coherent correlation between $^{87}Sr/^{86}Sr$ and $\delta^{18}O$ exists (Fig. 7f), and as independent evidence indicates significant variation in the primary $\delta^{18}O$ composition of the Akademikerbreen carbonates, we consider Sr concentrations as the most useful diagnostic tool for determining the fidelity of Sr isotope signatures. Samples with [Sr]>250 ppm are regarded here as faithful proxies for original seawater composition.

Insofar as this interpretation is correct, then our Sr isotope data through the Svanbergfjellet and Grusdievbreen formations (Fig. 8) show a limited variation from 0.70625 to 0.70660, consistent with the least radiogenic values documented in this stratigraphic interval by Derry et al. (1989). Scatter over a range of ~0.00025 is apparent, and may be the consequence of leaching of radiogenic Sr from clastic components during diagenesis or sample preparation (Derry et al., 1989). Bearing this intrinsic scatter in mind, we have identified subtle but distinct trends in the evolution of seawater $^{87}Sr/^{86}Sr$ through the Lower Akademikerbreen Group. First,

$^{87}Sr/^{86}Sr$ remains nearly constant at 0.70625 in the lower Grusdievbreen Formation, then rises to as high as 0.70660 above the G1 boundary (Fig. 8). This slight rise broadly coincides with a pulse of siliciclastic sediment input into the EGES basin (Fig. 4), raising the question of whether this signal could be the result of Sr in-growth from radiogenic Rb bound in clay minerals. However, these elevated $^{87}Sr/^{86}Sr$ ratios are also found in very pure, Sr-rich limestones in the upper part of the upper Grusdievbreen Formation, suggesting that this increase in $^{87}Sr/^{86}Sr$ is a primary signal. $^{87}Sr/^{86}Sr$ then declines gradually back to values near 0.70625 beneath the S1 boundary, and remains at this level into the lowermost limestones above the boundary. Limited data show a sharp rise up section in the Lower Limestone Member, but this trend needs to be confirmed with additional analyses.

## 5. Discussion

Previously published isotopic data from the Neoproterozoic succession in Svalbard showed low $\delta^{13}C$ values in the middle Akademikerbreen Formation (Knoll et al., 1986; Derry et al., 1989, 1992). We have confirmed these values and documented in detail the evolution of seawater $\delta^{13}C$ through the Grusdievbreen and Svanbergfjellet formations (Fig. 8). Several striking features of this record deserve mention. First, the negative isotope interval appears symmetrical to the first order, interrupting an overall trend of high $\delta^{13}C$ that characterizes the Akademikerbreen Group (Knoll et al., 1986; Halverson et al., 2005). The isotope interval is delineated by a sharp drop of 8‰ in $\delta^{13}C$ in the Grusdievbreen Formation and a similarly sharp rise of the same magnitude in the lower Svanbergfjellet Formation (Fig. 8). The most impressive feature of the $\delta^{13}C$ record is that both shifts correspond precisely to transient fluctuations in sea level that exposed the Akademikerbreen platform to subaerial erosion and karstification. No other major sequence boundaries occur within the Akademikerbreen Group.

Negative $\delta^{13}C$ anomalies are a hallmark feature of the Neoproterozoic. Whereas these anomalies were formerly ascribed solely to post-glacial cap carbonates (e.g. Kennedy, 1996; Kaufman and Knoll, 1995; Kaufman et al., 1997), recent studies have demonstrated that a >10‰ negative $\delta^{13}C$ anomaly preceded the Marinoan glaciation (McKirdy et al., 2001; Halverson et al., 2002, 2004). Likewise, it appears that a post-Marinoan glaciation is preceded by the most extreme drop in $\delta^{13}C$ in the Neoproterozoic (Halverson et al., 2005; Xiao et al., 2004). These findings have revealed that the relationship between the negative $\delta^{13}C$ anomalies and glaciation is not straightforward and is different for each event. Nevertheless, the association between the anomalies and glaciation remains. For this reason, we previously speculated that the negative isotope shift at the G1 boundary was a proxy for a cryptic glaciation (Halverson and Maloof, 2001). This hypothesis was reinforced by the similarity of the basal parasequence of the upper Grusdievbreen Formation to typical Marinoan cap–carbonate sequences. This upward-shoaling parasequence stands out amidst the background stratigraphy (Fig. 5a), contains reddened siliciclastic sediments (otherwise rare in the Akademikerbreen Group), and has a regionally extensive layer choked with seafloor cements, which are uncommon in the Neoproterozoic outside of Marinoan cap carbonates (Groztinger and Knoll, 1995). The combined isotopic and stratigraphic patterns above the G1 boundary are reminiscent of Marinoan cap–carbonate sequences, albeit without a cap dolostone.

On the other hand, the sequence above the S1 boundary resembles typical Sturtian cap–carbonate sequences, which lack a basal cap dolostone, are relatively rich in organic matter (or disseminated sulfides), and contain abundant sub-littoral, microbially-influenced sediments. The $\delta^{13}C$ trend in Sturtian cap carbonates includes negative values at their very base (Kennedy et al., 1998; Hoffman and Schrag, 2002; Yoshioka et al., 2003), but the anomaly is commonly base-truncated due to delayed deposition of the lower cap carbonate (Hoffman and Schrag, 2002; Halverson et al., 2005). Therefore, the Sturtian cap carbonate is most consistently distinguished isotopically by a sharp rise in $\delta^{13}C$ in the lower part of the cap–carbonate sequence. These stratigraphic and isotopic features are found in the strata overlying the S1 boundary, and it is possible that the black shales directly above the exposure surface could mask a basal negative $\delta^{13}C$ anomaly. However, for reasons discussed below, we believe this S1 boundary is not related to glaciation.

### 5.1. Global correlations

The G1 boundary clearly cannot correspond to the Marinoan glaciation as the Marinoan cap–carbonate sequence comprises the lower Dracoisen Formation of the Polarisbreen Group (Fig. 1; Halverson et al., 2005). But can the S1 surface correspond to the Sturtian glaciation? If our interpretation that both glacial diamictites in the Polarisbreen Group belong to the Marinoan glaciation (Halverson et al., 2005) is correct, then the Sturtian glaciation must be represented, if not directly by glacial deposits, then by a sedimentological and geochemical proxy for the cap carbonate (Knoll, 2000) somewhere in the stratigraphic section beneath the Petrovbreen Member diamictite (Fig. 1). Due to its association with a major $\delta^{13}C$

anomaly, it is tempting to speculate that the S1 boundary could be temporally equivalent to Sturtian glacial deposits found in other basins. No geochronological data is available to test directly this correlation. However, much indirect chemostratigraphic and stratigraphic evidence militates against this interpretation. For example, in no succession where unambiguous Sturtian age glacial deposits are found is the glaciation preceded by a prolonged interval of negative $\delta^{13}C$ values (Halverson et al., 2005) as is the S1 boundary. It cannot be ruled out that the negative isotope interval actually corresponds to the glaciation itself (implying that it was not a global glaciation) and has hitherto been undocumented. However, Sturtian glacial deposits commonly fill major erosional unconformities (Young, 1992), and the attendant fall in sea level would have precluded deposition of the Lower Dolomite Member, which was deposited in shallow water. Also, average $^{87}Sr/^{86}Sr$ (0.7063) in the Grusdievbreen and Svanbergfjellet formations is significantly lower than the value of ~0.7068 commonly associated with the Sturtian glaciation (Kaufman et al., 1997; Kennedy et al., 1998; Jacobsen and Kaufman, 1999; Shields, 1999; Walter et al., 2000; Yoshioka et al., 2003).

Perhaps the most compelling argument that the S1 boundary does not correspond to the Sturtian glaciation is the apparent correlation of the carbon isotopic record of the Grusdievbreen–Svanbergfjellet with that of the Bitter Springs Formation (Halverson et al., 2005), which lies stratigraphically well below the Sturtian age glacial deposits of the Aralka Formation in the Amadeus Basin of central Australia (Walter et al., 1995). Fig. 9 shows the Bitter Springs $\delta^{13}C$ data (Hill et al., 2000a) plotted along with the Svalbard data, scaled such that the negative and positive shifts align. Both the positive and negative shifts are equal in magnitude, and the isotopic pattern between the G1 and S1 boundaries is virtually identical to the $\delta^{13}C$ profile through the lower half of the Loves Creek Member (Hill et al., 2000a). $^{87}Sr/^{86}Sr$ data from the Bitter Springs Formation are rather variable and do not definitively corroborate this correlation. However, $^{87}Sr/^{86}Sr$ values as low 0.7057 occur in the Gillen Member (Hill et al., 2000a), and one test of this correlation will be whether similarly unradiogenic values occur in the lowermost Akademikerbreen Group.

This correlation enables a rough estimate of the age of the lower Akademikerbreen Group since age constraints in Australia are tighter than those in Svalbard. Hill et al. (2000a,b) previously argued that the upper Bitter Springs Formation is ~830 Ma based on correlation of volcanics in the upper Loves Creek Member with the 827±6 Ma Gairdner Dyke Swarm (Wingate et al., 1998) on the Gawler craton. However, a younger age seems more likely since the Bitter Springs Formation appears to correlate with the isotopically light Curdimurka Subgroup (Hill and Walter, 2000) in the Adelaide geosyncline (Preiss, 2000). If this correlation is correct, then the beginning and end of the negative $\delta^{13}C$ interval are broadly constrained to ca 800 Ma by the 802±10 Rook Tuff (Fanning et al., 1986) in the lower Curdimurka Subgroup and the 777±7 Ma Boucaut Volcanics (Preiss, 2000) in the lower Burra Group (Fig. 9).

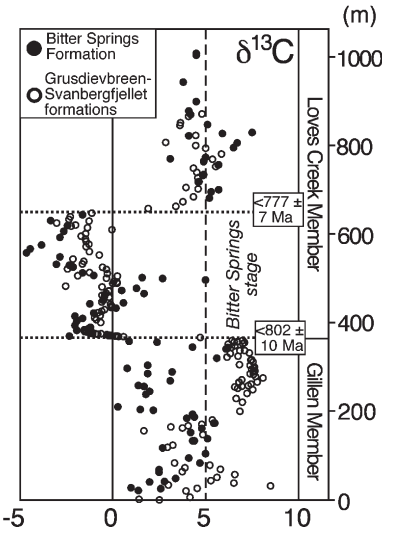


Fig. 9. Overlay of $\delta^{13}C$ data from the Bitter Springs Formation (Hill et al., 2000a) and data from the Grusdievbreen and Svanbergfjellet formations (from Fig. 3), scaled so as to match the negative and positive $\delta^{13}C$ shifts across the G1 and S1 boundaries. Note the nearly perfect match of $\delta^{13}C$ data within the Bitter Springs stage. The exception is a positive spike in the Bitter Springs Formation that corresponds to an interval of non-marine deposition (Hill et al., 2000a) and may not reflect a primary seawater signal. Approximate ages of G1 and S1 boundaries are taken from correlation of the Bitter Springs stage with the Callanna Group in the Adelaide Geosyncline, which is constrained by U–Pb ages on the Rook Tuff (Fanning et al., 1986) at the base of the Callanna Group (Preiss, 2000) and the Boucaut Volcanics at the base of the overlying Burra Group (Preiss, 2000).

Rainbird et al. (1996) correlated the Bitter Springs Formation with the upper part of the their "Succession B" in northern Canada based on lithological and stratigraphic similarities between the two continents. This correlation implies that the negative $\delta^{13}C$ interval should occur within the Little Dal Group in the Mackenzie Mountains and in the Shaler Supergroup and equivalent strata in the Amundsen Basin (Rainbird et al., 1996). A preliminary study has shown an interval of $^{13}C$-depleted carbonates in the Shaler Supergroup (Asmeron et al., 1991), while new data from the Mackenzie Mountains reveal a pronounced negative anomaly in the middle Little Dal Group that is most

likely correlative with the Bitter Springs anomaly in Svalbard and central Australia (Halverson, 2006).

### 5.2. The Neoproterozoic $^{87}Sr/^{86}Sr$ record

The combination of a distinct $\delta^{13}C$ pattern with nearly constant Sr-isotopic composition make the low $\delta^{13}C$ interval in the lower Akademikerbreen Group particularly well suited for global correlations. It is well established that seawater $^{87}Sr/^{86}Sr$ increased dramatically from unradiogenic values <0.7060 in the early Neoproterozoic to >0.7070 by the Marinoan glaciation (Veizer et al., 1983; Asmeron et al., 1991; Derry et al., 1992; Jacobsen and Kaufman, 1999; Shields, 1999; Walter et al., 2000; Melezhik et al., 2001; Thomas et al., 2004). However, as the comprehensive compilations of Neoproterozoic $^{87}Sr/^{86}Sr$ data by Melezhik et al. (2001) and Thomas et al. (2004) have revealed, the current database is contradictory and suggests highly variable seawater $^{87}Sr/^{86}Sr$, particularly in the middle Neoproterozoic. Several factors contribute to the confusing Neoproterozoic $^{87}Sr/^{86}Sr$ record. The combination of a lack of radiometric ages for this time interval, poorly constrained correlations, and inconsistent sample quality all result in artificial variation seen in composite Sr isotope records. Most compilations indicate that $^{87}Sr/^{86}Sr$ values as low as those in the Grusdievbreen and Svanbergfjellet formations (~0.7063) are restricted to carbonates older than ca 770 Ma (Melezhik et al., 2001; Thomas et al., 2004). However, Kuznetsov et al. (2003) suggest instead that $^{87}Sr/^{86}Sr$ remained below 0.7063 until ~650 Ma.

In their model on Neoproterozoic sedimentary cycling, Derry et al. (1992) argued that both the generally increasing $^{87}Sr/^{86}Sr$ and high $\delta^{13}C$ seawater compositions through the latter half of the Neoproterozoic reflected high rates of continental erosion and marine sedimentation, resulting in increased input of radiogenic Sr into the oceans and high fractional burial of organic carbon ($f_{org}=C_{organic\text{-}buried}/C_{total\text{-}buried}$). Even with the much greater residence time of Sr in the oceans compared to C, given the apparent longevity of the negative $\delta^{13}C$ interval in the Akademikerbreen Group, one would anticipate a decrease in $^{87}Sr/^{86}Sr$ if the drop in $\delta^{13}C$ was the result of decreased rates of continental erosion. Instead, $^{87}Sr/^{86}Sr$ rises slightly by ~0.0002 directly above the G1 sequence boundary and remains elevated (up to 0.70660) through most of the negative $\delta^{13}C$ interval (Fig. 8). Although it cannot be ruled out that the change in $^{87}Sr/^{86}Sr$ was related to a decrease in the input of hydrothermal Sr, the concurrence of the increase in $^{87}Sr/^{86}Sr$ with the input of siliciclastic sediments into the EGES basin and the decay of this subtle anomaly (Fig. 8) with the return to pure carbonate deposition suggest that it records a change in continental weathering patterns. However, since silicate weathering rates can only increase over long time scales with a concomitant increase in $CO_2$ outgassing rates, this pulse of radiogenic Sr into the oceans must have been related either to a transient elevation of $pCO_2$ or change in the average $^{87}Sr/^{86}Sr$ composition of weathered continental crust.

### 5.3. The $\delta^{18}O$ record

The significance of the $\delta^{18}O$ composition of ancient marine carbonates is a subject of much debate. On the one hand, the best-preserved Proterozoic limestones are consistently depleted by 5–8‰ when compared to Cenozoic values (Veizer and Hoefs, 1976; Burdett et al., 1990; Kah, 2000; Frank and Lyons, 2000). Similarly, $\delta^{18}O$ values of marine calcite, aragonite, and phosphate shells suggest a gradual rise in the $\delta^{18}O$ composition of the oceans from −8 to 0‰ through the Phanerozoic (Veizer et al., 1999). This argument is countered by modeling results (e.g. Muehlenbachs and Clayton, 1976; Muehlenbachs, 1998) and $\delta^{18}O$ analyses of silicate minerals in ophiolites of various ages (Gregory and Taylor, 1981; Holmden and Muehlenbachs, 1993), which suggest that seawater $\delta^{18}O$ is buffered against long-term change by hydrothermal circulation through mid-ocean ridges. However, these arguments disregard possible variations in the temperature at which crustal alteration occurs, which can drive long-term changes in marine $\delta^{18}O$ (Wallman, 2001) and also exert a dominant control on the $\delta^{18}O$ composition of altered oceanic crust. Although the purpose of this paper is not to try to resolve this controversy, our data are consistent with long term variation of marine $\delta^{18}O$ over geological time.

The oxygen isotopic trends spanning the G1 boundary underline the potential pitfalls in interpreting the $\delta^{18}O$ record of Neoproterozoic carbonates. Both the rise in $\delta^{18}O$ beneath the G1 boundary and the negative anomaly above it are highly reproducible in all measured sections. However, a combination of petrologic and geochemical evidence suggests that these two trends are the consequence of dolomitization and meteoric diagenesis, respectively. The fact that the dolomitization trend is preserved (Fig. 7a) despite the evidence for widespread groundwater flow reveals that these dolomite beds were relatively resistant to isotopic equilibration. The reproducibility of the meteoric signal in all measured sections (Fig. 4) is also impressive and suggests that the silty parasequence was at one time a basin-wide aquifer. Since this aquifer would have been disconnected by faulting and folding during Caledonian deformation, it is reasonable to

surmise that the meteoric signal is pre-Caledonian in age. The preservation of the discordant isotopic signals across the G1 boundary (Fig. 4) further suggests that the $\delta^{18}O$ composition of these rocks has not been appreciably modified in the past 400 Ma. These observations imply a high preservation potential for Svalbard limestones, despite isolated instances of extensive, pre-Caledonian meteoric diagenesis.

Dolomitization and meteoric diagenesis left distinct imprints on the elemental composition of Akademikerbreen carbonates (Fig. 7). Fig. 8 shows a compilation of the $\delta^{18}O$ composition of all samples spanning the G1 and S1 boundaries for which elemental data indicate minimal alteration (Mg/Ca, Mn/Sr < 0.1). Notably, both the positive deflection beneath the G1 boundary and the negative anomaly above it apparent in raw $\delta^{18}O$ data (Fig. 4) are absent from this compilation of least altered data. Interestingly, $\delta^{18}O$ in the best-preserved samples above the G1 boundary is roughly equal to or slightly higher than average $\delta^{18}O$ in the lower Akademikerbreen Group, whereas a decline in $\delta^{18}O$ of ~2‰ occurs below the exposure surface (Fig. 8). If this decline in $\delta^{18}O$ values represents a primary signal, then either it reflects a transient warming episode (~8 °C) or a freshening of the EGES basin. Given the geological evidence for the emergence and dolomitization of the Akademikerbreen platform, the latter hypothesis is unlikely. Since the downturn in $\delta^{13}C$ values also begins beneath the G1 boundary, it seems that the mechanism responsible for perturbing the global carbon cycle, and perhaps the warming of the EGES basin, preceded the nadir in sea level during which the G1 sequence boundary developed.

### 5.4. Evidence for True Polar Wander events?

The association of large shifts in the carbon-isotopic composition of Neoproterozoic seawater with regionally persistent sequence boundaries insinuates glaciation. However, indirect evidence for a pre-Sturtian age implies that the Bitter Springs isotope stage precedes any of the known Neoproterozoic ice ages. A ca 800–780 Ma glaciation cannot be ruled out, but no supporting evidence has been found in any basin of this age. Therefore, a different mechanism must be sought that can simultaneously account for the $\delta^{13}C$ pattern, the pair of relative sea level fluctuations, and enhanced continental weathering above the G1 sequence boundary, as indicated by both the influx of red silt and rise in $^{87}Sr/^{86}Sr$.

New paleomagnetic data from limestone and siltstone samples spanning the G1 boundary in the Grusdievbreen Formation and from the Upper Algal Dolomite Member in the Svanbergfjellet Formation add a key piece to this puzzle. These data (Maloof et al., 2006) will be discussed in greater detail in a separate paper, and only the results are summarized here (Fig. 8). A stable, high temperature magnetic component has been found in about 85% of a suite of samples collected from three different sections spanning the G1 boundary. This remnant magnetization is reproduced in all sections, is distinct from regional overprints of younger age from Svalbard, and passes a Caledonian fold test. Whereas the paleomagnetic inclination remains nearly constant (~15°), the declination changes by ~55° across the sequence boundary (Fig. 8). Paleomagnetic data from the Svanbergfjellet Formation, which pass a syn-sedimentary fold test, preserve a paleomagnetic declination similar to that beneath the G1 boundary, only with a slightly higher inclination.

The evidence for meteoric diagenesis above the G1 boundary raises the possibility that the paleomagnetic signature is an overprint signal. However, if primary, and assuming the geocentric axial dipole hypothesis is valid for the middle Neoproterozoic, then the 55° discordance in declination can only be accounted for by a large rotation of the EGES platform with respect to the earth's spin axis. Plate tectonics can produce such rotations, but a minimum of ~30 Ma is required to account for a rotation of this magnitude (Maloof et al., 2006). Given the conformable nature of the strata (Figs. 3, 5) and continuity of the $\delta^{13}C$ pattern (Fig. 8) across the sequence boundaries, this time span is inconsistent with the data.

Another mechanism capable of producing rotations of this magnitude is true polar wander (TPW), where the entire solid earth rotates with respect to the spin axis, which remains fixed in a celestial reference frame. Inertial interchange true polar wander (IITPW) is a variety of TPW in which mantle heterogeneities are arranged in such a way that a small redistribution of mass causes the solid earth to rotate by up to 90° (Fisher, 1974). During an IITPW event, continents furthest from the IITPW rotational axis will undergo large latitudinal shifts (paleoinclination), while those closest to the axis will undergo large rotations (paleodeclination) and little latitudinal change. The rate of rotation of the silicate earth during an IITPW event is limited by the relaxation time of Earth's hydrostatic bulge, and a full 90° rotation is estimated to require 3–20 Ma (Steinberger and O'Connell, 1997).

An IITPW event would also generate transient sea level changes related to the delayed response of the solid earth with respect to the ocean under gravitational load (Mound and Mitrovica, 1998; Mound et al., 1999). A continent traversing the equator would experience a relative rise in sea level as it moved to lower latitude and a relative fall in sea level as it moved to higher latitude, with

maximum effects at 45° from the IITPW axis. (Mound et al., 1999). Based on the position of the EGES platform with respect to a calculated IITPW axis, Maloof et al. (2006) estimated a relative fall in sea level change of up to 25 m during both the G1 and the S1 IITPW events. Since the transient fall in sea level would coincide with only a fraction of the total IITPW event, the low in sea level would endure less than ~3–20 m.y. (Steinberger and O'Connell, 1997). Therefore, a pair of IITPW events, which is consistent with the paleomagnetic data, could account for the G1 and S1 sequence boundaries.

Kirschvink et al. (1997) proposed an early Cambrian IITPW event and speculated that it contributed to the early radiation of metazoa. Kirschvink and Raub (2003) further hypothesized that a Cambrian IITPW event would trigger episodic releases of methane from marine clathrate reservoirs as a consequence of changes in ocean circulation (and therefore temperature) and sea level (pressure). Due to the highly $^{13}$C-depleted composition of methane (~−60‰; Kvenvolden, 1993), Kirschvink and Raub (2003) argued that these methane bursts could explain high order fluctuations in the early Cambrian $\delta^{13}$C record. Outbursts of this potent greenhouse gas to the oceans and atmosphere may help explain the $\delta^{18}$O data beneath the G1 boundary, which suggest warming of the EGES basin prior to exposure of the carbonate platform. The pulse of increased silicate weathering could also be related to this warming event, but another possible explanation is that during the IITPW rotation, Laurentia and other low-latitude continents traversed new climatic regimes, which could have changed the loci of continental weathering and destabilized the landscape (cf. Zhang et al., 2001) over vast areas. The input of methane-derived carbon and decrease in biological removal of carbon from the oceans could account for the increased alkalinity implied by the formation of seafloor cements above the G1 boundary. However, methane alone cannot account for the low $\delta^{13}$C values between the G1 and S1 boundaries as the volume of methane required to suppress marine $\delta^{13}$C by ~8‰ through ~325 m of carbonate far outstrips the potential global reservoir of methane clathrate (Buffet, 2000; Dickens, 2001). Another more fundamental change to global carbon cycling is required.

The most straightforward way to alter seawater $\delta^{13}$C for extended intervals of time is to change the fractional burial of organic carbon in marine sediments ($f_{org}$; Kump and Arthur, 1999). The ~8‰ decline across the G1 boundary could be accounted for by a shift in $f_{org}$ from ~0.35 to 0.15. Organic carbon burial is mainly determined by a combination of sedimentation rates and primary productivity, the latter of which is controlled by nutrient supply and both of which are tied to continental weathering (Schrag et al., 2002). Today, approximately 70‰ of total organic carbon removed from the biosphere is buried in large tropical river deltas (Hedges and Keil, 1995). Schrag et al. (2002) postulated that a preponderance of continents in low latitudes would have maintained high $f_{org}$ and therefore the high $\delta^{13}$C characteristic of much of the Neoproterozoic (Knoll et al., 1986) as a consequence of a large number of tropical rivers and more restricted equatorial ocean basins in which bottom-water anoxia would facilitate burial of organic matter and nutrient recycling. An IITPW event in the middle Neoproterozoic (G1) would have rotated those equatorial continents and basins far from the IITPW axis into higher latitudes, reducing the number of large tropical rivers (Maloof et al., 2006) and exposing previously restricted basins to zonal ocean currents, thereby increasing mixing and inhibiting the development of anoxic conditions. The consequence of such an event would be a reduction in global carbon burial rates and a decrease in $\delta^{13}$C to a new steady state controlled by the new distribution of the continents. Likewise, a second (S1) IITPW event during which the continents returned to their equatorial positions would boost organic carbon burial and drive $\delta^{13}$C back up to the typical high Neoproterozoic values. Therefore, at least qualitatively, a pair of IITPW events could account for the large, symmetric $\delta^{13}$C shifts at the G1 and S1 boundaries.

A proposed connection between the negative $\delta^{13}$C interval and an IITPW event is admittedly speculative. However, Li et al. (2004) have independently proposed a TPW event occurring sometime between ~800 and 750 Ma to explain disparate paleopoles from South China, and suggest that it drove a mantle superswell and associated ca. 800 Ma flood basalts from polar to tropical latitudes. Determining whether the Li et al. (2004) TPW event is synchronous with the Akademikerbreen low $\delta^{13}$C interval and consistent with the proposed G1 and S1 IITPW events will require additional geochronological and chemostratigraphic constraints. However, our IITPW hypothesis is straightforward to test because the relative sea level changes and paleomagnetic disparities associated with an IITPW event are different but predictable for every continent (Mound et al., 1999; Evans, 2003), given a particular paleogeography.

## 6. Conclusions

We have presented detailed stratigraphic and chemostratigraphic data spanning a salient interval of low $\delta^{13}$C in the middle Akademikerbreen Group in northeast Svalbard. We estimate this interval to be ca 800 Ma based on the correlation with the lower Loves Creek Member of the Bitter Springs Formation in central Australia, which has a

virtually identical $\delta^{13}C$ trend (Fig. 9; Hill et al., 2000a). Insofar as this correlation is correct, then this isotopic anomaly is global and preceded the Sturtian glaciation. The symmetry of the $\delta^{13}C$ anomaly suggests that the positive and negative shifts that define its beginning and end represent transitions between distinct stable states of global organic carbon burial. A slight rise in seawater $^{87}Sr/^{86}Sr$ above the G1 boundary implies that $f_{org}$ and erosion rates were not directly coupled. However, the coincidence of the $\delta^{13}C$ shifts with major sequence boundaries point to a connection to global phenomena that were capable of affecting regional sea level, patterns of organic carbon burial, and weathering patterns on the continents.

Given the association between large negative $\delta^{13}C$ anomalies and glaciation in the Neoproterozoic (Knoll et al., 1986), it is tempting to associate the Akademikerbreen negative $\delta^{13}C$ interval to a pre-Sturtian glaciation that has hitherto been undocumented. However, the absence of any direct evidence for glaciation in Svalbard, central Australia, and other presumably coeval sedimentary successions (e.g. in northern Canada) demands an alternative explanation. New paleomagnetic data from Svalbard (Maloof et al., 2006) may provide the answer. These data indicate a rapid 55° rotation of the EGES platform spanning the G1 boundary and a counter rotation of approximately the same magnitude across the S1 boundary. We propose that a pair of IITPW events can account for both the paleomagnetic data and the transient changes in relative sea level at the G1 and S1 sequence boundaries. The low $\delta^{13}C$ values that occur between these two sequence boundaries could be accounted for by dramatically altered patterns of organic carbon burial (cf. Schrag et al., 2002) between the two IITPW events resulting from changes in nutrient delivery and ocean circulation patterns. Although this hypothesis is speculative, it is straightforward to test since the Akademikerbreen $\delta^{13}C$ anomaly should be easy to identify in carbonates of equivalent age, and the paleomagnetic and eustatic imprints of an IITPW event are variable but predictable for other continents, based on their position relative to the IITPW axis (Mound et al., 1999; Evans, 2003). If subsequent paleomagnetic studies support the evidence from Svalbard for a pair of IITPW events ca 800 Ma, the associated shifts in steady state marine $\delta^{13}C$ composition will be testament to the profound effect of paleogeography on global carbon cycling.

## Acknowledgments

This work was supported by the National Science Foundation (Arctic Science Program grant OPP-9817244 to Paul Hoffman, Harvard University), the NASA Astrobiology Institute, the Canadian Institute for Advanced Research (Earth System Evolution Project), and a GSA graduate research grant to GPH. We thank Alcides Sial for inviting GPH to submit this manuscript. Constructive reviews by Ján Veizer and Andrey Bekker greatly improved the quality of the manuscript. Paul Hoffman supervised and funded the field project in Svalbard, which was carried out as part of GPH's and ACM's PhD research. Sam Bowring supervised strontium isotope analyses at MIT. Andy Knoll provided much insight and many suggestions on fieldwork and related manuscripts. Norsk Polarinstitutt provided logistical support in Svalbard. Winfried Dallman and Ken Petersen helped organize fieldwork. Ethan Goddard and Greg Eischeid provided assistance and supervision in stable isotopic and elemental analyses.

## Appendix A. Supplementary data

Supplementary data associated with this article can be found, in the online version, at doi:10.1016/j.chemgeo.2006.06.013.

## References

Asmeron, Y., Jacobsen, S.B., Knoll, A.H., Butterfield, N.J., Swett, K., 1991. Strontium isotopic variations of Neoproterozoic seawater: implications for crustal evolution. Geochim. Cosmochim. Acta 55, 2883–2894.

Bailey, T.R., McArthur, J.M., Prince, H., Thirlwall, M.F., 2000. Dissolution methods for strontium isotope stratigraphy: whole rock analysis. Chem. Geol. 167, 313–319.

Banner, J.L., Hanson, G.N., 1990. Calculation of simultaneous isotopic and trace element variations during water–rock interaction with applications to carbonate diagenesis. Geochim. Cosmochim. Acta 54, 3123–3137.

Bowring, S., Myrow, P., Landing, E., Ramezani, J., Grotzinger, J., 2003. Geochronological constraints on terminal Proterozoic events and the rise of Metazoans. Geophys. Res. Abstr. (EGS, Nice) 5, 13219.

Brand, U., Veizer, J., 1980. Chemical diagenesis of a multicomponent carbonate system-1: trace elements. J. Sediment. Petrol. 50, 1219–1236.

Brand, U., Veizer, J., 1981. Chemical diagenesis of a multicomponent carbonate system-2: stable isotopes. J. Sediment. Petrol. 51, 987–997.

Brasier, M., McCarron, G., Tucker, R., Leather, J., Allen, P., Shields, G., 2000. New U–Pb zircon dates for the Neoproterozoic Ghubrah glaciation and for the top of the Huqf Supergroup, Oman. Geology 28, 175–178.

Buffet, B., 2000. Clathrate hydrates. Annu. Rev. Earth Planet. Sci. 28, 477–507.

Burdett, J.W., Grotzinger, J.P., Arthur, M.A., 1990. Did major changes in the stable-isotope composition of Proterozoic seawater occur? Geology 18, 227–230.

Demicco, R.V., Hardie, L.A., 1994. Sedimentary structures and early diagenetic features of shallow marine carbonate deposits. SEPM Atlas Ser. 1 264 pp.

Derry, L.A., Keto, L.S., Jacobsen, S.B., Knoll, A.H., Swett, K., 1989. Sr isotopic variations in Upper Proterozoic carbonates from Svalbard and East Greenland. Geochim. Cosmochim. Acta 53, 2331–2339.

Derry, L.A., Kaufman, A.J., Jacobsen, S.B., 1992. Sedimentary cycling and environmental change in the Late Proterozoic: evidence from stable and radiogenic isotopes. Geochim. Cosmochim. Acta 56, 1317–1329.

Dickens, G., 2001. The potential volume of ocean methane hydrates. Org. Geochem. 32, 1132–1193.

Evans, D.A.D., 2003. True polar wander and supercontinents. Tectonophysics 362, 303–320.

Fairchild, I.J., Hambrey, M.J., 1984. The Vendian succession of northeastern Spitsbergen: petrogenesis of a dolomite–tillite association. Precambrian Res. 26, 111–167.

Fairchild, I.J., Hambrey, M.J., 1995. Vendian basin evolution in East Greenland and NE Svalbard. Precambrian Res. 73, 217–233.

Fairchild, I.J., Spiro, B., 1987. Petrological and isotopic implications of some contrasting Late Precambrian carbonates, NE Spitsbergen. Sedimentology 34, 973–989.

Fairchild, I.J., Hambrey, M.J., Spiro, B., Jefferson, T.H., 1989. Late Proterozoic glacial carbonates in northeast Spitsbergen: new insights into the carbonate–tillite association. Geol. Mag. 126, 469–490.

Fanning, C.M., Ludwig, K.R., Forbes, B.G., Preiss, W.V., 1986. Single and multiple grain U–Pb zircon analyses for the early Adelaidean Rook Tuff, Willouran Ranges, South Australia. Abstr. Geol. Soc. Aust. 15, 71–72.

Fisher, D., 1974. Some more remarks on polar wandering. J. Geophys. Res. 79, 4041–4045.

Frank, T.D., Lyons, T., 2000. The integrity of $\delta^{18}O$ records in Precambrian carbonates: a Mesoproterozoic case study. In: Grotzinger, J.P., James, N.P. (Eds.), Carbonate Sedimentation and Diagenesis in the Evolving Precambrian World. SEPM Spec. Pub., vol. 67. Society for Sedimentary Geology, Tulsa, pp. 315–326.

Gee, D.G., Page, L.M., 1994. Caledonian terrane assembly on Svalbard: new evidence from $^{40}Ar/^{39}Ar$ dating in Ny Friesland. Am. J. Sci. 294, 1166–1186.

Gee, D.G., et al., 1995. Grenvillian basement and a major unconformity within the Caledonides of Nordaustlandet, Svalbard. Precambrian Res. 70, 215–234.

Gregory, R.T., Taylor, H., 1981. An oxygen isotope profile in a section of Cretaceous oceanic crust, Samail Ophiolite, Oman: evidence for $\delta^{18}O$ buffering of the oceans by deep (5 km) seawater hydrothermal circulation at mid-ocean ridges. J. Geophys. Res. 86, 2737–2755.

Groztinger, J.P., Knoll, A.H., 1995. Anomalous carbonate precipitates: is the Precambrian the key to the Permian? Palaios 10, 578–596.

Halverson, G., 2006. A Neoproterozoic Chronology. In: Xiao, S., Kaufman, A. (Eds.), Neoproterozoic Geobiology and Paleobiology. Topics in Geology, vol. 27. Springer, New York, pp. 231–271.

Halverson, G.P., 2003. Towards and integrated stratigraphic and carbon isotopic record for the Neoproterozoic. PhD thesis, Harvard University, Cambridge, MA, 276 pp.

Halverson, G.P., Maloof, A.C., 2001. Isotopic and stratigraphic evidence for a cap carbonate in the Neoproterozoic Grusdievbreen Formation, northeastern Svalbard (abstract). European Union of Geosciences (Proceedings), Strasbourg, p. A101.

Halverson, G.P., Hoffman, P.F., Schrag, D.P., Kaufman, A.J., 2002. A major perturbation of the carbon cycle before the Ghaub glaciation (Neoproterozoic) in Namibia: prelude to snowball Earth? Geochem. Geophys. Geosyst. 3, doi:10.1029/2001GC000244.

Halverson, G.P., Maloof, A.C., Hoffman, P.F., 2004. The Marinoan glaciation (Neoproterozoic) in northeast Svalbard. Basin Res. 16, 297–324.

Halverson, G.P., Hoffman, P.F., Schrag, D.P., Maloof, A.C., Rice, A.H., 2005. Towards a Neoproterozoic composite carbon isotopic record. Geol. Soc. Amer. Bull. 117, 1181–1207.

Harland, W.B., Gayer, R.A., 1972. The Arctic Caledonides and earlier oceans. Geol. Mag. 109, 289–314.

Harland, W.B., Scott, R.A., Aukland, K.A., Snape, I., 1992. The Ny Friesland Orogen, Spitsbergen. Geol. Mag. 129, 679–707.

Harland, W.B., Hambrey, M.J., Waddams, P., 1993. Vendian Geology of Svalbard, vol. 193. Norsk Polarinstit, Skrift. 150 pp.

Hartz, E.H., Torsvik, T.H., 2002. Baltica upside down: a new plate tectonic model for Rodinia and the Iapetus Ocean. Geology 30, 255–258.

Hedges, J., Keil, R., 1995. Sedimentary organic-matter preservation—an assessment and speculative synthesis. Mar. Chem. 49, 81–115.

Hill, A.C., Walter, M.R., 2000. Mid-Neoproterozoic (~830–750 Ma) isotope stratigraphy of Australia and global correlation. Precambrian Res. 100, 181–211.

Hill, A.C., Arouri, K., Gorjan, P., Walter, M.R., 2000a. Geochemistry of marine and nonmarine environments of a Neoproterozoic cratonic carbonate/evaporite: the Bitter Springs Formation, Central Australia. In: Grotzinger, J.P., James, N.P. (Eds.), Carbonate Sedimentation and Diagenesis in the Evolving Precambrian World. SEPM Spec. Pub., vol. 67. Society for Sedimentary Geology, Tulsa, pp. 327–344.

Hill, A.C., Cotter, K.L., Grey, K., 2000b. Mid-Neoproterozoic biostratigraphy and isotope stratigraphy in Australia. Precambrian Res. 100, 281–298.

Hoffman, P.F., Schrag, D.P., 2002. The snowball Earth hypothesis: testing the limits of global change. Terra Nova 14, 129–155.

Hoffman, P.F., Kaufman, A.J., Halverson, G.P., Schrag, D.P., 1998a. A Neoproterozoic snowball. Earth Sci. 281, 1342–1346.

Hoffman, P.F., Kaufman, A.J., Halverson, G.P., 1998b. Comings and goings of global glaciations on a Neoproterozoic tropical platform in Namibia. GSA Today 8 (5), 1–9.

Hoffmann, K.-H., Condon, D.J., Bowring, S.A., Crowley, J.L., 2004. A U–Pb zircon date from the Neoproterozoic Ghaub Formation Namibia: constraints on Marinoan glaciation. Geology 32, 817–820.

Holmden, C., Muehlenbachs, K., 1993. The $^{18}O/^{16}O$ ratio of 2-billion0year-old seawater inferred from ancient oceanic crust. Science 259, 1733–1736.

Jacobsen, S.B., Kaufman, A.J., 1999. The Sr, C, and O isotopic evolution of Neoproterozoic seawater. Chem. Geol. 161, 37–57.

Johannson, Å., Larianov, A.N., Tebenkov, A.M., Gee, D.G., Whitehouse, M.J., Vestin, J., 2000. Grenvillian magmatism of western and central Nordaustlandet, northeastern Svalbard. Trans. R. Soc. Edinb. 90, 221–234.

Kah, L.C., 2000. Depositional $\delta^{18}O$ signatures in Proterozoic dolostones: constraints on seawater chemistry and early diagenesis. In: Grotzinger, J.P., James, N.P. (Eds.), Carbonate Sedimentation and Diagenesis in the Evolving Precambrian World. SEPM Spec. Pub., vol. 67. Society for Sedimentary Geology, Tulsa, pp. 345–360.

Kaufman, A.J., Knoll, A.H., 1995. Neoproterozoic variations in the C-isotopic composition of seawater: stratigraphic and biogeochemical implications. Precambrian Res. 73, 27–49.

Kaufman, A.J., Hayes, J.M., Knoll, A.H., Germs, G.J.B., 1991. Isotopic compositions of carbonates and organic carbon from upper Proterozoic successions in Namibia: Stratigraphic variation and the effects of diagenesis and metamorphism. Precambrian Res. 49, 301–327.

Kaufman, A.J., Knoll, A.H., Narbonne, G.M., 1997. Isotopes, ice ages, and terminal Proterozoic earth history. Proc. Natl. Acad. Sci. 94, 6600–6605.

Kennedy, M.J., 1996. Stratigraphy, sedimentology, and isotopic geochemistry of Australian Neoproterozoic postglacial cap dolostones: deglaciation, $\delta^{13}C$ excursions, and carbonate precipitation. J. Sediment. Res. 66, 1050–1064.

Kennedy, M.J., Runnegar, B., Prave, A.R., Hoffman, K.H., Arthur, M., 1998. Two or four Neoproterozoic glaciations? Geology 26, 1059–1063.

Kirschvink, J., Raub, T., 2003. A methane fuse for the Cambrian explosion. Compt. Rend. Geosci. 335, 65–78.

Kirschvink, J., Ripperdan, R., Evans, D., 1997. Evidence of a large-scale reorganization of Early Cambrian continental masses by inertial interchange true polar wander. Science 277, 541–545.

Knoll, A.H., 2000. Learning to tell Neoproterozoic time. Precambrian Res. 100, 3–20.

Knoll, A.H., Swett, K., 1987. Micropaleontology across the Precambrian–Cambrian boundary in Spitsbergen. J. Palaeontol. 61, 898–926.

Knoll, A.H., Swett, K., 1990. Carbonate deposition during the late Proterozoic era: an example from Spitsbergen. Am. J. Sci. 290-A, 104–132.

Knoll, A.H., Hayes, J.M., Kaufman, A.J., Swett, K., Lambert, I.B., 1986. Secular variation in carbon isotope ratios from Upper Proterozoic successions of Svalbard and east Greenland. Nature 321, 832–837.

Knoll, A.H., Swett, K., Burkhardt, E., 1989. Paleoenvironmental distribution of microfossils and stromatolites in the upper Proterozoic Backlundtoppen Formation, Spitsbergen. J. Paleontol. 63, 129–145.

Knoll, A.H., Swett, K., Mark, J., 1991. Paleobiology of a Neoproterozoic tidal flat/lagoonal complex: the Draken Formation, Spitsbergen. J. Paleontol. 65, 531–570.

Knoll, A.H., Walter, M.R., Narbonne, G.M., Christie-Blick, N., 2004. A new period for the geologic time scale. Science 305, 621–622.

Kuznetsov, A., Semikhatov, M., Gorokhov, I., Melnikov, N., Konstantinova, G., Kutyavin, E., 2003. Sr isotopic composition in carbonates of the Karatau Group, southern Urals, and standard curve of $^{87}Sr/^{86}Sr$ variations in the Late Riphean ocean. Strat. Geol. Correlation 11, 415–449.

Kump, L.R., Arthur, M.A., 1999. Interpreting carbon-isotope excursions: carbonates and organic matter. Chem. Geol. 161, 181–198.

Kvenvolden, K., 1993. Gas hydrates—geological perspective and global change. Rev. Geophys. 31, 173–187.

Land, L.S., 1980. The isotopic and trace element geochemistry of dolomite: the state of the art. In: Zenger, D.H., Dunham, J.B., Ethington, R.L. (Eds.), Concepts and Models of Dolomitization. SEPM, Tulsa, pp. 87–111.

Larianov, A., Gee, D.G., Tebenkov, A.M., Witt-Nillson, P., 1998. Detrital zircon ages from the Planetfjella Group of the Mosselhalvøya Nappe, NE Spitsbergen, Svalbard. International Conference on Arctic Margins III, Celle (Germany), pp. 109–110.

Li, Z.X, Evans, D.A.D., Zhang, S., 2004. A 90° spin on Rodinia: possible causal links between the Neoproterozoic supercontinent, superplume, true polar wander and low-latitude glaciation. Earth Planet. Sci. Lett. 220, 409–421.

Lyberis, N., Manby, G., 1999. Continental collision and lateral escape deformation in the lower and upper crust: an example from Caledonide Svalbard. Tectonics 18, 40–63.

Maloof, A.C., Halverson, G.P., Kirschvink, J.L., Schrag, D.P., Weiss, Benjamin P., Hoffman, P.F., 2006. Combined paleomagnetic, isotopic, and stratigraphic evidence for true polar wander from the Neoproterozoic Akademikerbreen Group, Svalbard. Geol. Soc. Amer. Bull. 118, 1099–1124.

McKirdy, D.M., Burgess, J.M., Lemon, N.M., Yu, X., Cooper, A.M., Gostin, V.A., Jenkins, R.J.F., Both, R.A., 2001. A chemostratigraphic overview of the late Cryogenian interglacial sequence in the Adelaide Fold–Thrust Belt, South Australia. Precambrian Res. 106, 149–186.

Melezhik, V.A., Gorokhov, I.M., Kuznetsov, A.B., Fallick, A.E., 2001. Chemostratigraphy of Neoproterozoic carbonates: implications for 'blind dating'. Terra Nova 13, 1–11.

Mound, M.E., Mitrovica, J.X., 1998. True polar wander as a mechanism for second-order sea level fluctuations. Science 279, 534–537.

Mound, M.E., Mitrovica, J.X., Evans, D.A.D., Kirschvink, J.L., 1999. A sea-level test for inertial interchange true polar wander events. Geophys. J. Int. 136, F5–F10.

Muehlenbachs, K., 1998. The oxygen isotopic composition of the oceans, sediments, and the seafloor. Chem. Geol. 145, 263–273.

Muehlenbachs, K., Clayton, R.N., 1976. Oxygen isotope composition of the oceanic crust and its bearing on seawater. J. Geophys. Res. 81, 4365–4369.

Preiss, W.V., 2000. The Adelaide Geosyncline of South Australia and its significance in Neoproterozoic continental reconstruction. Precambrian Res. 100, 21–63.

Rainbird, R.H., Jefferson, C.W., Young, G.M., 1996. The early Neoproterozoic sedimentary succession B of northwestern Laurentia: correlations and paleogeographic significance. Geol. Soc. Amer. Bull. 108, 454–470.

Schrag, D.P, Berner, R., Hoffman, P.F., Halverson, G.P., 2002. On the initiation of snowball Earth. Geochem. Geophys. Geosyst. 300, doi:10.1029/2001GC000219.

Shields, G., 1999. Working towards a new stratigraphic calibration scheme for the Neoproterozoic–Cambrian. Eclogae Geol. Helv. 92, 221–233.

Shields, G., Veizer, J., 2002. Precambrian marine carbonate isotope database: version 1.1. Geochem. Geophys. Geosyst. 3, doi:10.1029/2001GC000266.

Steinberger, B., O'Connell, R., 1997. Changes of the Earth's rotation axis owing to advections of mantle density heterogeneities. Nature 387, 169–173.

Thomas, C.W., Graham, C.M., Ellam, R.M., Fallick, A.E., 2004. $^{87}Sr/^{86}Sr$ chemostratigraphy of Dalradian limestones of Scotland and Ireland: constraints on depositional ages and time scales. J. Geol. Soc. (Lond.) 161, 229–242.

Torsvik, T., Lohman, K., Sturt, B., 1996. Vengian glaciations and their relation to the dispersal of Rodinia: paleomagnetic constraints. Geology 23, 727–730.

Veizer, J., Hoefs, J., 1976. The nature of $^{18}O/^{16}O$ and $^{13}C/^{12}C$ secular trends in sedimentary carbonate rocks. Geochim. Cosmochim. Acta 40, 1387–1395.

Veizer, J., Compston, W., Clauer, N., Schidlowski, M., 1983. $^{87}Sr/^{86}Sr$ in Late Proterozoic carbonates: evidence for a 'mantle event' at 900 Ma. Geochim. Cosmochim. Acta 47, 295–302.

Veizer, J., Ala, D., Azmy, K., Bruckschen, P., Buhl, D., Bruhn, F., Carden, G.A.F., Diener, A., Ebneth, S., Godderis, Y., Jasper, T., Korte, C., Pawellek, F., Podlaha, O.G., Strauss, H., 1999. $^{87}Sr/^{86}Sr$, $\delta^{13}C$ and $\delta^{18}O$ evolution of Phanerozoic seawater. Chem. Geol. 161, 59–88.

Wallman, K., 2001. The geological water cycle and the evolution of marine $\delta^{18}O$. Geochem. Cosmochim. Acta 65, 2469–2485.

Walter, M.R., Veevers, J.J., Calver, C.R., Grey, L., 1995. Neoproterozoic stratigraphy of the Centralian Superbasin, Australia. Precambrian Res. 73, 173–195.

Walter, M.R., Veevers, J.J., Calver, C.R., Gorjan, P., Hill, A.C., 2000. Dating the 840–544 Ma Neoproterozoic interval by isotopes of strontium, carbon, and sulfur in seawater, and some interpretative models. Precambrian Res. 100, 371–433.

Williams, G.E., 1979. Sedimentology, stable-isotope geochemistry and palaeoenvironment of dolostones capping late Precambrian glacial sequences in Australia. J. Geol. Soc. Aust. 26, 377–386.

Wilson, C.B., 1958. The lower Middle Hecla Hoek rocks of Ny Friesland, Spitsbergen. Geol. Mag. 95, 305–327.

Wilson, C.B., 1961. The upper Middle Hecla Hoek rocks of Ny Friesland, Spitsbergen. Geol. Mag. 98, 89–116.

Wingate, M.T.D., Campbell, I.H., Compston, W., Gibson, G.M., 1998. Ion microprobe U–Pb ages for Neoproterozoic basaltic magmatism in south-central Australia and implications for the breakup of Rodinia. Precambrian Res. 87, 135–159.

Xiao, S., Bao, H., Wang, H., Kaufman, A.J., Zhou, C., Li, G., Yuan, X., Ling, H., 2004. The Neoproterozoic Quruqtagh Group in eastern Chinese Tianshan: evidence for a post-Marinoan glaciation. Precambrian Res. 130, 1–26.

Yoshioka, H., Asahara, Y., Tojo, B., Kawakami, S., 2003. Systematic variations in C, O, and Sr isotopes and elemental concentrations in Neoproterozoic carbonates in Namibia: implications for glacial to interglacial transition. Precambrian Res. 124, 69–85.

Young, G.M., 1992. Late Proterozoic stratigraphy and the Canada–Australia connection. Geology 20, 215–218.

Zhang, P., Molnar, P., Downs, W.R., 2001. Increased sedimentation rates and grain sizes 2–4 Myr ago due to the unfluence of climate change on erosion rates. Nature 410, 891–897.